Online characterization of viscoelastic and

stress-relaxation behavior in thermoforming

by

Iman Rezazadeh-Bahadoran

Department of Mechanical Engineering

McGill University, Montreal

August 2005

A thesis submitted to McGill University in partial fulfillment of

the requirements of the degree of

Masters in Engineering

Canada

Abstract

The thermoforming process is subject to a lot of variability with regard to the viscoelastic properties of the material, and the level of residual stresses caused by the manufacturing (extrusion and calandering) process of a plastic sheet. A robust control system must be able to identify and adjust to these perturbations in real time during the thermoforming process.

The research project proposes two process sub-models, which predict the behavior of the elastic modulus and the level of frozen-in stresses. These two sub-models will be used in a model based control system, consisting of a number of process sub-models encompassing different material properties and machine characteristics.

A series of experiments was conducted using an industrial thermoforming machine to measure the elasticity and the level of frozen-in stresses in the material. A bubble inflation technique was used to determine the behavior of the elastic modulus in the transition state between solid and liquid. Additionally, a simulation of the sag that occurs during plastic sheet heating was developed to identify the level of frozen-in stresses.

Résumé

Le procédé de thermoformage induit beaucoup de variabilité dans les propriétés viscoélastiques du matériau ainsi que dans le niveau de contraintes résiduelles causés par le procédé de fabrication (extrusion et calandrage) de la feuille de plastique. Un système de contrôle robuste doit être capable d'identifier et de s'ajuster à ces perturbations en temps réel pendant le procédé de thermoformage.

Le projet de recherche décrit dans la présentation propose deux sous-modèles du procédé qui prédisent le comportement du module élastique ainsi que le niveau de contraintes gelées. Ces deux sous-modèles seront utilisés dans un système de contrôle basé sur modèle consistant en plusieurs sous-modèles du procédé et couvrant plusieurs propriétés du matériau ainsi que des caractéristiques de la machin.

Une série d'expériences furent effectuées sur une machine de thermoformage industrielle afin de mesurer l'élasticité ainsi que le niveau de contraintes gelées dans le matériau. Une technique de gonflement de bulle a été utilisée pour déterminer le comportement du module élastique dans la zone de transition entre l'état liquide et solide. De plus une simulation de l'affaissement (sag) qui se produit pendant le réchauffement de la feuille a été mise au point pour identifier le niveau de contraintes gelées.

Contents

List of Tables

List of Figures

1. Introduction

Thermoforming is a process in which useful parts are manufactured by forming a flat sheet of plastic material. The thermoforming process consists of three basic phases:

1) Sheet heating, where a flat plastic sheet is heated throughout its thickness inside an oven, until it reaches a temperature between the minimum and maximum forming temperature.

2) Forming, where the sheet is formed to the profile of a mold by using pressure and/or vacuum in order to achieve the desired final part shape.

3) Cooling, where the part is cooled in the mold until the formed material solidifies and is rigid enough to be removed.

This thesis mostly focuses on the heating stage of thermoforming process. In the simplest control technique, the control process tries to produce uniform sheet temperature distribution prior to forming. Non-uniform sheet temperature distributions can result in localized webbing and non-uniform thickness in the finished part. In many cases, there is a maximum and minimum temperature constraint that needs to be realized across a sheet and disrespecting these constraints will generally result in rejected parts.

There are two main phenomena that have to be considered when designing a robust control system for sheet heating. The first phenomenon is the heat transfer by both absorption of the sheet and the energy provided by the heating elements. The second phenomenon which is the subject of this thesis is the rheological behavior of the sheet during the heating stage. This includes the viscoelastic behavior of the material and the relaxation of residual stresses inside the sheet.

Most of the materials used for the thermoforming process are semi-crystalline polymers with different viscoelastic properties. Knowledge of the variations of these properties is very important in modeling and controlling the process as they greatly impact sheet heating near the melting point.

Also the level of frozen-in stresses varies from batch to batch. Even two polymer sheets from the same batch can have different levels of frozen-in stresses, which are caused by extrusion and calendering processes during manufacturing. Sheet sag is directly related to the manufacturing process, and is a critical parameter for the control of thermoforming. Relaxation of frozen-in stresses can reduce sag as the sheet heats up and the material goes above the transition temperature. This results in shrinkage of the sheet after the relaxation process. Sheet sag also directly effects the flux level applied to the sheet as the distance between the sheet and heating elements is changing during heating stage. This especially applies in the thermoforming of thick sheets, such as HDPE, where the high molecular weight increases the memory effect.

Therefore, controlling sheet heating is a very critical issue for thermoforming applications. The goal of this research project is to develop an online technique which is capable of detecting and characterizing the viscoelastic properties and the amount of frozen-in stresses inside a plastic sheet prior to forming. In order to characterize the viscoelastic properties of the material, the behavior of the elastic modulus during the whole thermoforming process is considered and simulated. Also, in order to characterize the amount of frozen-in stresses inside the sheet, a close measurement of sag is conducted and simulated. Proper characterization of material mechanical properties and their variations is a pre-requisite to improve the productivity of the thermoforming process.

The specific objectives of this online technique for the thermoforming process are defined by the constant need for productivity improvement in the industrial environment. The most basic motivation is lower rejects, which will increase production efficiency and significantly decrease material costs. This is particularly important for the producers of products manufactured from very expensive plastic materials.

Also higher quality parts can be achieved through better control of material distribution during forming. Additionally production efficiency can be improved by decreasing the manufacturing cycle time for each part. By characterizing the mechanical properties of the sheet during the heating stage, the capacity of a simulation to predict the most efficient heating time can be increased. In other words, this technique can lead to multifaceted increases in production rates.

Many new methods are explored in this research. The bubble formation technique is used to characterize the viscoelastic properties in the transition region between the solid and liquid state of the material, which is the most important region for the forming operation. The bubble inflation technique is one of the experiments that yield important information on the relationship between the rate of deformation and the shear strain for biaxial membrane stretching. In this technique a free bubble is formed by applying pressure to the pre-heated sheet. The Monark thermoforming machine at the Industrial Materials Institute (IMI) facility was used along with proper sensors. The experiments and analysis are described in detail later in the thesis.

This thesis has been carried out in cooperation with the Industrial Materials Institute (IMI), an institute of the National Research Council of Canada, located in Boucherville, Québec, Canada. The IMI conducts research and development activities

with an emphasis on materials and their application to forming and process control. This thesis research was conducted with the Modeling and Diagnostics Section of IMI, where major efforts are invested in developing process simulation and modeling tools.

The fact that there has been very little work done on online control of the thermoforming process is a direct outcome of the historically conservative nature of the thermoforming industry. In comparison, much more work on process modeling and control has been done for blow molding and especially for injection molding. Simulation software has long been used to improve and speed up the development and process control of injection molded parts. The thermoforming industry is, however, catching up. Although the implementation of closed-loop control is not yet established, the use of thermoforming simulation software during product design is increasing. A number of simulation packages are now commercially available. T-Sim from Accuform is recognized as one of the first simulation packages available to thermoformers. C-Mold, which offers the popular Moldflow injection molding simulation software, also has a thermoforming simulation package. Other simulation packages are offered by Fluent Inc. and ESI Group Sherwood Technologies is in the process of developing Java based programs for the simulation of sheet heating and cooling only.

However in order to be effective simulation software has to take into account the absorptive of the material. The FormSim simulation software for thermoforming which has been developed at IMI by the intelligent forming team is such a package. FormSim can predict with good accuracy, the temperature map and internal temperature profile that is required for modern specialty materials. However, there are still a number of problems to be addressed before a simulation can be efficiently integrated into process control. One

of the main issues is the fact that material properties used in the simulation are not measured at actual operating conditions and can vary from batch to batch. Addressing these material related issues was the main motivation of conducting this research study.

FormSim allows users to simulate the various stages of the thermoforming process. As the demand for thermoforming simulation software increases, so too will the demand for increased accuracy of the simulated prediction. Therefore, an outcome of this research will be the provision of technique to identify online and update the material property data used by the simulation in order to improve the precision of the prediction of the FormSim simulation software.

A more detailed description of the thermoforming process and a description of IMI thermoforming equipment are given in chapter 2. Chapter 3 details methods used to characterize the viscoelastic properties of thermoformed materials, including a summary of the state of the art in the literature and some of the most recognized approaches to this problem. In chapter 4, techniques for quantifying the level of frozen-in stresses are presented. A summary of different approaches, as well as characterization of heating sag is proposed. Chapter 6 presents a summary and conclusions.

2. Description of Thermoforming Process

2.1. Introduction and Historical Review

Thermoforming is a generic term used to classify the many different techniques for producing useful articles from a planar thermoplastic sheet. The name thermoforming suggests the application of heat. Although this is true in general, there are particular forming techniques that do not require heat; however, for simplicity, the application of heat will be assumed throughout the remainder of this discussion.

The general idea behind the thermoforming process is not new. Even early man used heat to shape different organic materials into practical tools. However, the real roots of thermoforming came with the development of synthetic rubber during WWII. A variety of thermoplastic materials soon followed and consequently the thermoforming industry was born. The commercial success of thermoforming began in the late 1940's and early 50's with the development of the packaging industry. By the 60's blister packaging developed into a high volume market. The 60's also saw new advances and trends in the industry as well as the establishment of separate thin and thick sheet sectors [1]. During this time resin manufactures became more involved and offered technical support and expert knowledge of material properties to Thermoformers. By the 70's thermoforming machine manufacturers also began to support the advance of thermoforming technology. Demand had risen considerably in a few short years, which prompted machine manufacturers to develop high output equipment.

As the production volume increased in various thermoforming operations, the desire to cut costs prompted machine manufacturers to make advances in production and

quality control which led to more automated operations. The need to stay competitive and reduce costs also prompted improvements in scrap handling. Minimization of material costs and recycling suddenly became important issues. The 80's saw an even greater demand for more cost effective, automated operations. This led to further advances in thermoforming technology and allowed Thermoformers to introduce new product lines that were previously not possible. The 80's also saw the beginning of new pellet-to-product equipment as well as major advances in process control. The advance of thermoforming technology has not been continuous however. The industry saw a significant slowdown in the early 90's as a result of the economic slowdown in North America as well as the consequence of rising environmental concerns, which led to many fast food organizations discontinuing the use of certain types of takeout food containers. As a result, some product lines were discontinued, many thermoforming operations were left idle and a good number had to shut down completely.

Nowadays, the thermoforming industry is seeing growth once again. The comparatively low capital costs associated with the thermoforming process has derived interest in the possibility that advances in technology may allow new thermoforming techniques to manufacture many common parts, traditionally manufactured by other more expensive processes.

Even though considerable advances have been made in thermoforming since the beginning years, the industry, as a whole, has been relatively conservative in terms of the application of new technologies when compared to other polymer processing industries. For instance, the injection molding industry has long used FEM simulation software in the design and production of new parts. Because thermoforming is still considered to be a

process based on high craftsmanship and experience, it is regarded as the polymer processing area with the most growth potential. Advances in materials and process controls allow more complex parts to be made. For instance, twin-sheet thermoforming is now becoming the process of choice for manufacturing gas tanks that meet the strict Partial Zero Emissions Vehicle (PZEV) mandate that has been newly introduced in California. Also, the forming of very strong, lightweight foamed material is forecasted to continue to increase.

Similar to injection molding, thermoforming will likely see more automation and shorter product development times with the aid of various CAE tools. As heating costs continue to increase it is realistic to believe that strides will be taken towards improved, energy efficient thermoforming processing. Also, rises in material costs will see a continued effort to decrease the amount of waste associated with thermoforming. No one can say for certain exactly where the thermoforming industry will be 10 years from now; however, one can be certain in saying that the future certainly looks quite promising.

Advantages and Disadvantages

Some products can only be produced by one specific method, but there are many products in the polymer processing industry that can be manufactured by a number of different processes. Thermoforming has many competitive advantages when compared to other competing processes, low cost tooling and equipment is the most significant. In particular, the molds used for thermoforming are relatively simple and cheap compared to other forming processes. A further advantage of thermoforming is that it can handle multi-layered materials, foams, printed, and coated materials which can reduce the

amount of post-forming processing time. Finally, thermoforming can allow for the production of much larger parts than other processes. Thermoforming has however some drawbacks. Primarily, the low level of attainable details, limits the complexity of thermoformed products. Secondly, thermoforming process is a relatively high waste process, which causes higher material costs. Fortunately, some of the waste can be recycled. Finally, one of the other major drawbacks is the fact that only certain materials can be used in the thermoforming process.

Thermoforming Products

Having started with the production of simple tub-shaped parts for packaging purposes, today, the thermoforming industry supports a very large range of products with varying complexity. Many thermoformed parts that are in use today are produced to replace earlier forms of the same products that were made from different materials. Usually, plastic is much more durable, or it has other desirable material characteristics (i.e., thermal, electrical, chemical, etc.). Table 2.1 shows the diversity of thermoforming products in different industries [2].

Table 2.1: List of Thermoforming Products

Packaging and related items	Vehicular
Blister packs, point-or-purchase containers Bubble packs slip sleeve, vacuum carded containers Electronics audio/video cassette holders Tool cases hand, power Cosmetics cases, packages Foams meat, poultry trays Unit serving-foodstuffs Convenience: carry-out, cooking-box trays	Automotive door inner liners, headliners Automotive utility shelves, liners Automotive instrument panel skins Aircraft cabin wall panels, overhead compartment doors Snowmobile shrouds, windshields Motorcycle windshields, faring, scooter shrouds, mudguards All-terrain vehicle exterior components Golf cart shrouds, seats, trays

Convertible: oven food serving trays Wide-mouth jars Vending machine hot drink cups Cold drink cups- beer. soda Egg cartons Wine bottle protectors Produce separators-apples, grapefruit Portion medical unit dose Form-fill-seal-jelly, crackers, nuts and bolts	Tractor shrouds, door fascia Camper hardtops, interior components such as doors, cabinet tops Truck cab door fascia, instrument cluster fascia Recreational vehicle interior components, window blasters
Industrial	***Bulletins products***
Tote bins Pallets, single deck, double deck Parts trays, transport trays Equipment cases	Shutters, window fascia Skylights, translucent domes Exterior lighting shrouds Storage modules bath, kitchen, pantry Bath and shower surrounds, GR-UPE backed Soaking tubs, GR-UPE backed Retrofit shower components, shower trays
Others	
Exterior signs Advertising signs, lighted indoor signs Swimming and wading pools Tray, baskets, hampers, carrying cases Luggage Gun cases, golf club cases Boat hulls, surf-boards, with PUR foams Animal containers Prototype concepts for other plastic processes	

2.2. Physical Description of the Process

A comprehensive understanding of the thermoforming process and its different components is required in order to propose a successful control strategy. Therefore, the process is described here in a fair amount of detail. Thermoforming can usually be described as five simple and basic steps, but as J.l.Throne points out in his well-known book: "Thermoforming is not an easy process. It just looks easy" [3].

These five steps are:

10

- Clamping

- Heating

- Shaping or forming

- Cooling

- Trimming.

Clamping is the procedure of fixing and securing the sheet in order to pass through all the stages. In the heating stage the sheet is heated inside the oven up to a specific range of temperature also known as the forming window. In shaping, the sheet is formed on a mold using pressure and/or vacuum. Sometimes mechanical assistance through the use of drawers or slides is required. Then, the formed sheet is left to cool until it is firm enough to be removed from the mold. The formed sheet is then transferred to a trimming station for the removal of any excess material. All these steps are discussed in more details in this chapter.

2.2.1. Thermoforming Steps

2.2.1.1 Clamping the Sheet

The cut plastic sheet must be securely positioned in a frame for transport into the heating section and then back to the forming area. The frame must hold the sheet tight enough to prevent it from pulling free during the mechanical stretching that takes place during the forming cycle, and the thermal stress during heating. The clamping may be done manually or pneumatically. A manually operated toggle clamp performs acceptably for short production runs. Pneumatic clamping is a method best suited to larger production runs.

11

2.2.1.2 Heating the Sheet

The plastic sheet can be heated to its forming temperature by conduction, convection or radiation. Contact heaters heat the plastic sheet by conduction. In this case, the plastic sheet is held in contact with a uniformly heated metal plate, until its temperature matches that of the heated surface. Contact heaters are preferred for thin gauge sheets, where precise control of temperature distribution is required. In gas fired heaters, hot air is used to heat the sheet by convection. Here, the heated air is blown and forced by blowers and fans into a large oven which contains the clamped panel of plastic. Gas fired heaters are used for large and heavy gauge parts, since this is the most cost effective way to heat parts requiring large amounts of energy. Heating with radiant energy essentially uses infrared-light-spectrum wavelengths. When these waves are radiated towards the sheet, they will be transmitted and absorbed throughout the sheet in the case of infrared transparent plastics, which will heat it up. If the plastic sheet is colored these waves will heat its surface and then through conduction the interior of the sheet will get heated. Radiant heaters are the most preferred type of heaters because of their high energy efficiency and good temperature control [4].

The important factors to be considered when heating a sheet are: the uniformity of heating, the rate of heating, the sag and expansion of the plastic sheet, and the forming temperature range [5]. A uniform temperature distribution across the sheet to get uniform thickness distribution in the part is required. In some cases, a specific temperature profile across the sheet might be required to get the optimum thickness distribution in the final part.

12

The rate of heating depends on the sheet material, sheet thickness, and on whether the heating time determines the overall cycle time [5]. When the rate of heating is low, the temperature at the center of the sheet is nearly the same as the temperature at the surface; however, if the rate of heating is very high, there will be a large temperature gradient across the thickness of the sheet [6]. Sheets with a narrow temperature differential across the sheet thickness stretch uniformly and give parts with good thickness distribution and mechanical properties. If the sheet is heated too fast, then the surface of the sheet might reach its degradation temperature, while the center of the sheet is still below the forming temperature, resulting in rejected parts [5].

Upon heating, the thermoforming sheet undergoes changes in dimension. Initially, as the temperature of the sheet increases, it expands due to thermal expansion and may begin to show ripples or even sags. When the temperature of the sheet reaches its softening temperature, the residual stresses in the sheet due to the extrusion process are relaxed and the sheet shrinks. This causes tautness in the sheet and potential slip if not clamped properly. On further heating the sheet enters its elastic domain and sags under its own weight. If the sheet sag is not controlled, the sheet may come in contact with the lower heater and be thermally damaged [7].

Each thermoplastic material has a thermoforming range or forming window within which it can be stretched and formed properly. The lower thermoforming limit is the lowest temperature at which the material can still be molded with sufficient detail definition. The higher thermoforming limit is the temperature at which acceptable parts without damage can be formed. Damage may consist of surface burns, color changes, bubbles, tearing of the surface or excessive sheet sag [7].

2.2.1.3 Forming

Once the plastic sheet reaches its forming temperature, it is ready to be stretched and formed [8]. To stretch the hot pliable sheet and shape it into the contours of the mold some kind of force is necessary. Vacuum, air pressure, mechanical aids such as plugs, rubber diaphragms, and combinations of these are used to form the sheet against the mold surface. The type of forming force used depends on the size of the part, number of parts to be made, cycle speeds, the material to be molded, the mold material, and the thermoforming equipment [9].

Once the sheet touches the mold surface during stretching, it stops deforming [10]. As a result, the part is thicker in the areas where the sheet touches the mold wall first and thinner where it touches last. For applications, such as blister and bubble packs, where the extent to which the sheet is stretched is small, simpler methods of forming like vacuum forming or drape forming can be used. For applications, such as drinking cups, where the extent of stretching is large, pre-stretching of the sheet is required to ensure uniform thickness.

Forming methods can be divided into two types: one step forming and multi-step forming. One step forming includes drape forming, vacuum forming, pressure forming and free blowing. Multi-step forming includes forming techniques such as billow drape forming, billow vacuum forming, vacuum snap-back forming, plug assisted vacuum forming, plug assisted pressure forming, plug assisted drape forming, and reverse draw forming with plug assist [10]. Some of these techniques are discussed in detail later.

2.2.1.4. Sheet Cooling

Cooling of the sheet starts as soon as the sheet comes out of the heating oven. The sheet loses heat though conduction, convection, and radiation during the pre-stretching and forming stages. The cooling is more intense at the end of the forming stage, when the sheet comes in contact with the mold. Cooling time is a function of the following factors: type of polymer, material thickness after stretching, forming temperature, de-molding temperature, material of the thermoforming mold, temperature of the thermoforming mold, and contact between the formed part and the mold [11].

Different plastic materials have different thermal properties. Plastics with high specific heat and low thermal conductivity take longer to cool. The cooling time of a part is directly proportional to its thickness, i.e., the thinner the wall thickness after stretching, the quicker is the cooling. The article can be de-molded only after the area with the thickest cross section has sufficiently cooled. The higher the forming temperature, the longer the time required to cool the part to its demolding temperature, which is usually just below the T_g of the material or its deflection temperature under load (DTUL). The cooling time also depends on the mold material. Shorter cooling times can be achieved with molds having high thermal conductivity, such as aluminum. Good contact between the sheet and the tool is also required for faster cooling. Poor contact can occur if air is trapped between the sheet and the mold [11].

2.2.1.5. Trimming the Part

After the forming cycle is completed, the formed part must be separated from the surrounding material. Most thermoforming processes start with an expensive material; so, the trimming loses should be kept to a minimum [12]. When the thermoformed parts are

15

trimmed from the surrounding material, they leave behind a skeleton-like trim. This trim can be divided into two categories. One is the area surrounding the finished product called the edge trim. This includes the area used for clamping the sheet and the portion of the sheet used as a buffer between the actual clamping area and forming area. The other trim is called the space trim and this is the area between the molds in multi-cavity molding. Usually 10 to 40 % of the sheet material is trimmed [13].

Trimming of the part from the surrounding area must be done without distortion, damage, cracking or tearing of the part. The trimming must be dimensionally acceptable and done quickly enough to meet production requirements. The type of trimming equipment can range from a simple hand held knife to the most sophisticated laser beam cutting equipment [13]. If the trimming operation is done with electrically heated dies or when the sheet is hot, smoother cuts are obtained. High production parts are frequently trimmed in the forming mold itself. When the equipment does not have the ability to stack the parts immediately after trimming, then the parts should be left connected to the trim by narrow links to prevent the parts from getting stuck in the mold [12].

2.2.2. Thermoforming Techniques

There are many variations of the basic thermoforming method. These variations were developed to either improve the forming technique or to improve the finished product. Some of the techniques were developed to form materials impossible to form by conventional techniques. The main purpose in developing a new technique is to obtain better material distribution and better stretching of the material in the finished part [14]. Some of the forming techniques are discussed below.

2.2.2.1 Vacuum Forming

In vacuum forming a concave mold is used and air is removed from the area between the mold and the sheet as shown in Figure 2.1. As the air is evacuated between the mold and the sheet, atmospheric pressure forces the hot pliable sheet into the contours of the mold. This method is used for shallow articles, since the sheet thins out in deeply drawn parts. This method produces a part with thick side walls and thin bottoms [15].

Factors to be considered during vacuum forming are: adequate sealing between the sheet and the mold, the volume of the space to be evacuated, and the force required to form the part. There should be a good seal between the mold and the sheet as any leakage can cause a drop in the vacuum force, resulting in parts with poor detail. Vacuum pump volume capacity should always match the volume of the part to be evacuated. High vacuum forces with large parts can be achieved by using surge tanks. A surge tank is a source of vacuum, which is evacuated by a small volume pump. The vacuum in the surge tank is continuously replenished by the pump [16].
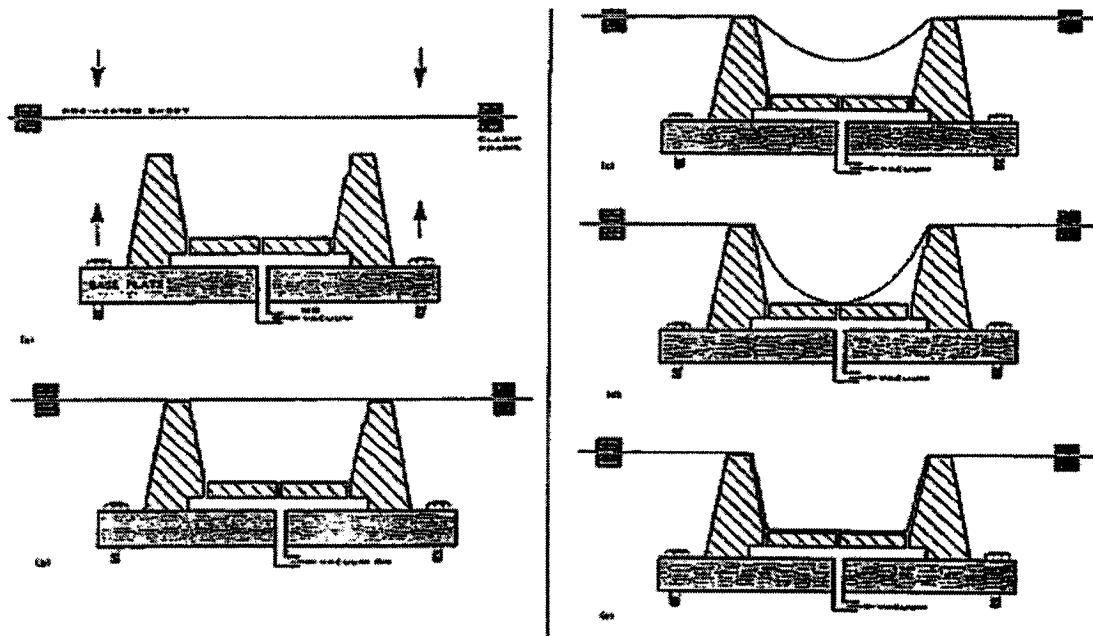
Figure 2.1: Thermoforming sequence for vacuum forming [17]

17

2.2.2.2. Pressure Forming

In vacuum forming, the maximum force available is atmospheric pressure. In order to produce parts with greater detail and with higher forming speeds, the pressure must be increased. This can be accomplished by pressure forming, which uses additional pressures (0.2 to 0.7 MPa) to form the part. Figure 2.2 shows the pressure forming technique.

Factors to be considered in pressure forming are: the material used for the construction of the mold, the venting of the mold, the seal between the pressure box and mold, and the pressure force required. The mold should be strong enough to withstand the forming forces. Cast aluminum and machined metal tooling are the preferred mold materials. Leakage in the seal between the pressure box and the mold will cause a reduction in the pressure force, resulting in poor part definition. In most cases the hot sheet acts as the seal, but sealants may be used in some cases. The sealants should be capable of withstanding the pressure forces. The venting at the bottom of the cavity should allow rapid evacuation of the mold when the pressure is applied. If the size of the vent holes is too small, the number of holes is insufficient, or the placement of the vent holes is not correct, it may result in trapped air. The trapped air does not allow the hot sheet to conform to the mold contours and this results in parts which are distorted. The pressure used for forming is very critical.

If the pressure is too low, the result is parts with poor definition, whereas higher pressures may cause distortion of the parts because there is not enough time for the evacuation of the mold. High pressures may even cause separation of the two platens, resulting in leakage [18].

18
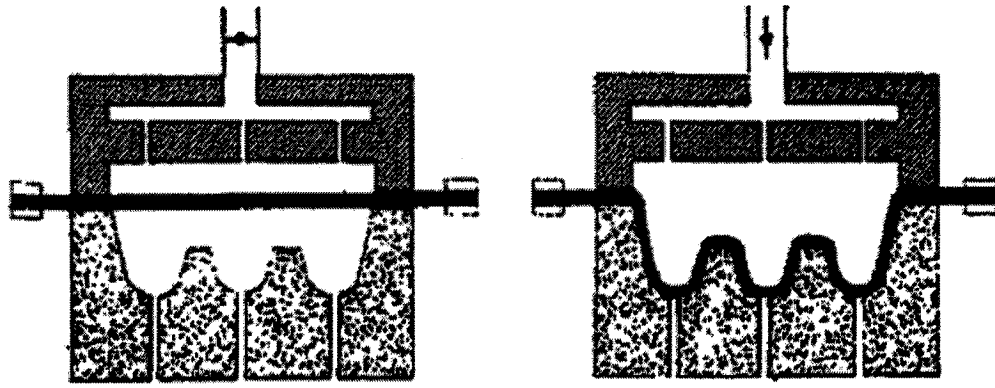
Figure 2.2: *Thermoforming sequence for pressure forming [19.]*

2.2.2.3. Free, Billow or Bubble Forming

In this method the heated sheet is sealed against a vacuum box and the vacuum is drawn as shown in Figure 2.3. The pressure differential causes the sheet to bulge inwards. The vacuum must be carefully controlled to repeatedly get the same shape. Only the depth of draw and shape of the perimeter can be varied in this forming method. This technique is primarily used to produce transparent parts, such as skylights, as the sheet does not come into contact with the mold [15].
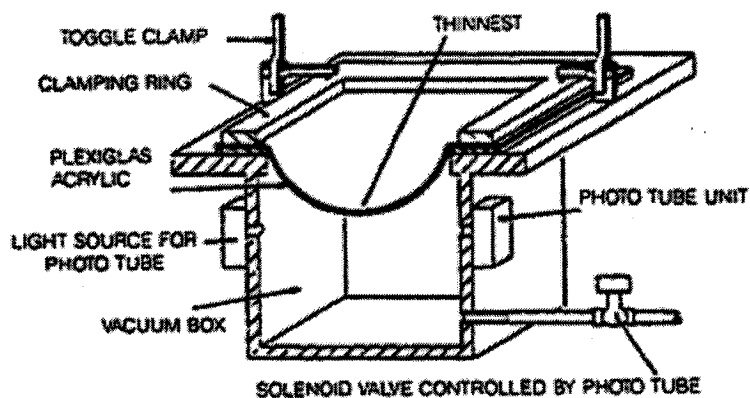
Figure 2.3: *Free blowing with vacuum [15]*

2.2.2.4 Drape Forming

Figure 2.4 shows the drape forming method where the heated sheet is formed against a male mold. In contrast to straight cavity forming this method gives parts with a thick bottom, and the sheet tends to thin out in the flange area. Good surface finish is obtained on the inside of the part [15].
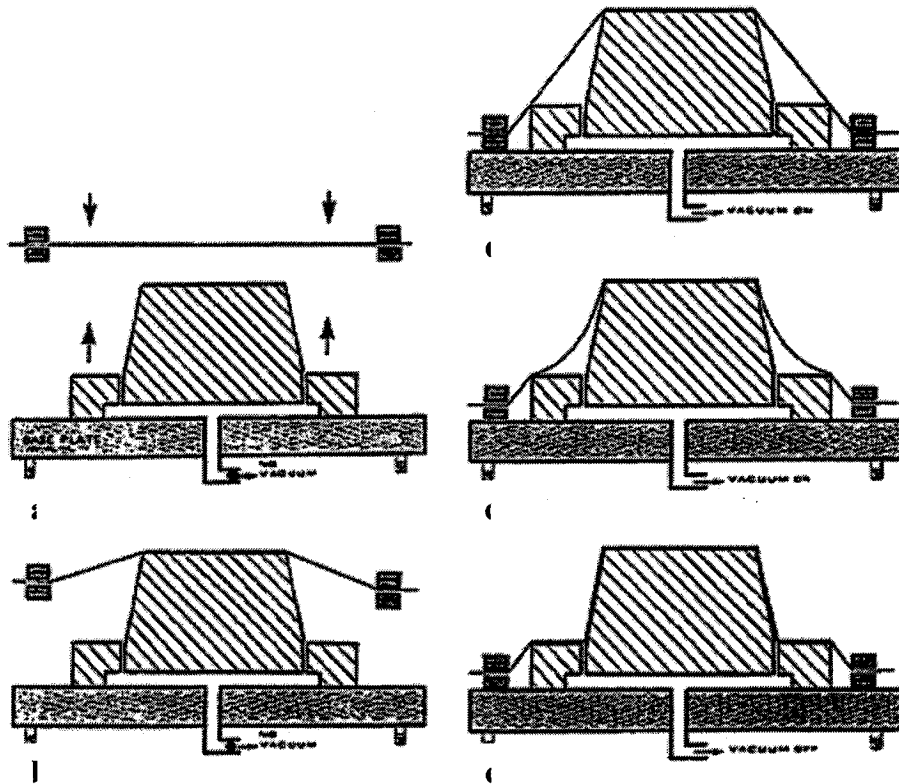
Figure 2.4: Thermoforming sequence for drape forming [21]

2.2.2.5. Plug Assist Forming

Plug assist thermoforming is the most widely used technique at present. The majority of the deep-draw containers are thermoformed by this technique. In plug assist thermoforming a mechanical assist is used to stretch and push the heated thermoplastic sheet before it touches the mold. This mechanical assist is called a plug. The plug

contacts the sheet first and stretches it until the plug is close to the bottom of the cavity. Then, air between the sheet and the mold is evacuated to accomplish the final forming [21]. Friction between the plug and the sheet has the effect that more material gets drawn into the base of the formed part. Draw ratio is defined as the ratio of the depth of the cavity to the minimum dimension at the rim of the cavity. With draw ratios of more than 1:3 in negative forming, plug assist is required [22].

Figure 2.5 shows the forming sequence for plug assist thermoforming where both pressure and vacuum are applied to form the part.
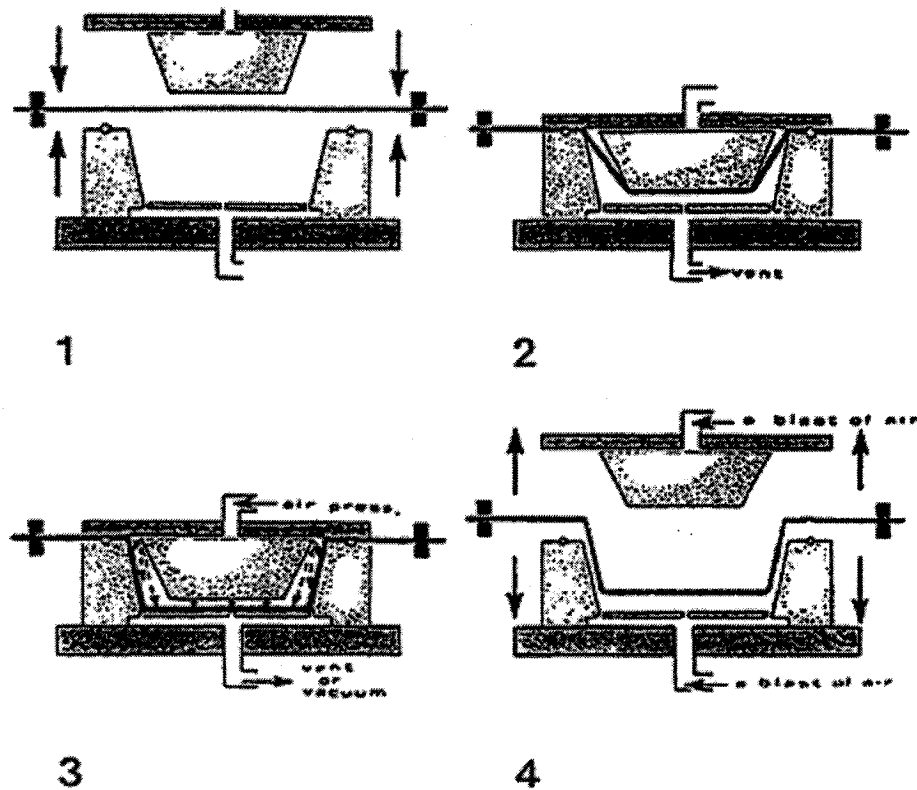
Figure 2.5: Forming sequence for plug assisted forming [23]

21

The shape of the plug is similar to that of the cavity, but is somewhat smaller. The size of the plug might be seven eighths or as small as three quarters the size of the cavity. The size difference results in a plug-like appearance of the assist in relation to the female cavity, and hence, the name "plug-assist". The use of plug assist provides very good material distribution in the parts; as a result draw ratios greater than 1:1 are possible. With the help of plug-assist, the material distribution of the part can be made so precise that hardly any difference can be observed in the wall thickness of the formed part.

2.2.2.6 Billow Drape Forming (Reverse Draw Technique)

In this technique the heated sheet is first sealed against the pressure box and then a bubble is formed by air pressure as shown in Figure 2.6. This results in pre-stretching of the sheet. Then, the male mold is pushed against the bubble and air is simultaneously vented from the chamber. When the plug reaches its final position, the sheet completely drapes the mold. Final forming is achieved by applying vacuum through the mold side. Better distribution of material is achieved by using this method [15].
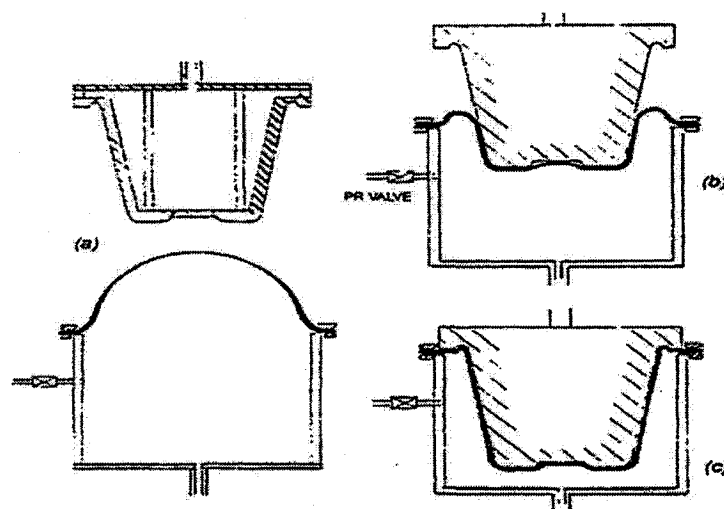
Figure 2.6: Forming sequence for billow drape forming [15].

22

2.2.2.7 Snap Back Forming

In snap back forming the heated sheet is sealed against the vacuum box and vacuum is drawn to form the bubble as shown in Figure 2.7. This method differs from the billow drape forming in that that the bubble is concave instead of convex, and the male mold does not push against the bubble. As the male mold reaches its bottom position, vacuum is released and the sheet snaps back on the male mold. Vacuum is applied from the mold side to complete the forming. This method eliminates the problem of chill marks, often observed in the billow drape forming technique [15].
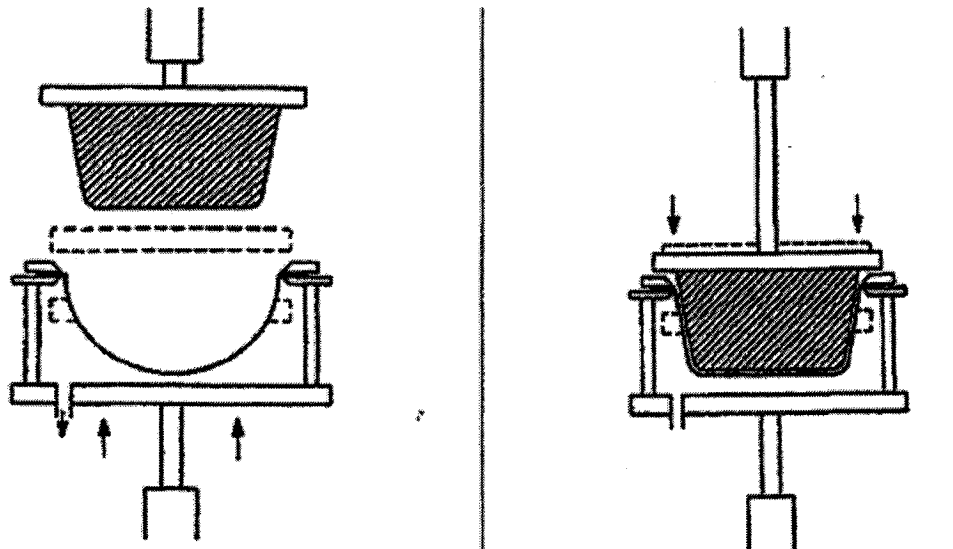
Figure 2.7: Forming sequence for snap back forming [24]

2.2.2.8 Reverse Draw with Plug-Assist Forming

This technique is a variation of the billow drape forming technique. In this method very precise control of the material distribution can be made by varying the size of the bubble, adjusting plug penetration and by control of plug temperature. In this method, a bubble is first blown upward by air pressure and is then stretched by the plug. After the plug reaches its set position, pressure is switched off and vacuum is applied [15]. This method is illustrated in Figure 2.8.
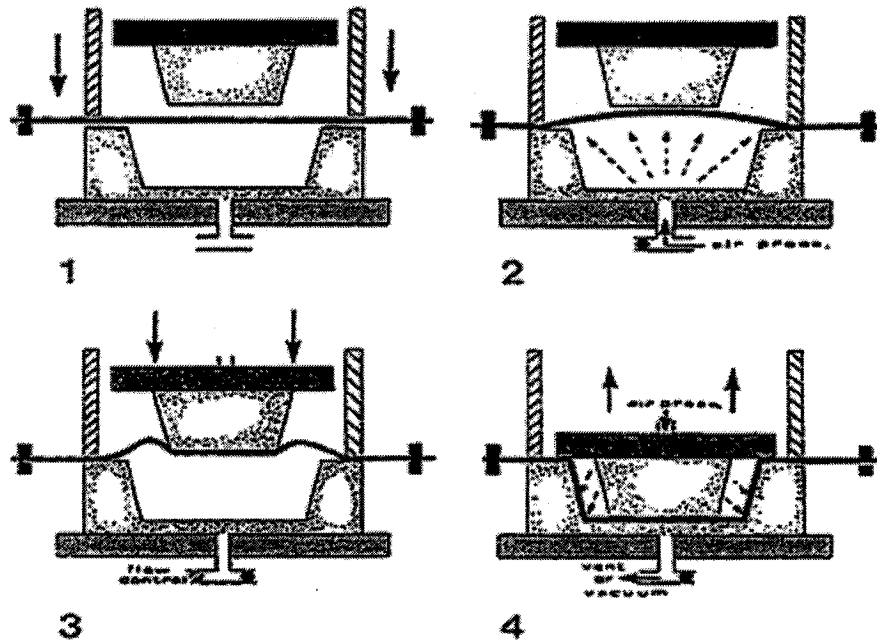
Figure 2.8: *Forming sequence for reverse draw with plug-assist forming [25]*

The reverse draw with plug assist forming is the technique that was used for conducting the related experiments in this research study. The main reason for choosing this technique was the need for studying the bubble inflation phenomena as a necessary part of the research.

2.3. IMI Equipment Description

All of the experimental measurements were performed on a Monark industrial scale thermoforming machine located at the IMI facility. This machine can perform standard, twin sheet and pressure forming. Table 2.2 shows general specifications of Monark thermoforming press.

Table 2.2: Monark's general specifications

Clamping Force	200 Tons
Maximum Oven Temperature	500 °C
Maximum Sheet Size	1.8 m x 1.8m

Following is a more detail description of the ovens and also the installed sensors in different section of Monark machine.

2.3.1. Ovens

Monark thermoforming machine is equipped with two ovens A and B, for doing twin sheet thermoforming. Oven B was equipped and used for conducting the related experiments in this research project. This oven has two heater banks with ceramic elements for profiled control of twenty four zones per side. Figure 2.9 and table 2.2 shows more details about the heater banks.

Table 2.3: *Specifications of Monark's oven B*

Heating Zone	X	Y
Dimension (mm):	1270	1796
Number of zones:	5	18
Gap between zones (mm):	10	40

BOTTOM ZONE AYOUT

TOP ZONE LAYOUT

Temperature_(oC)

375.0000
371.2500
367.5000
363.7500
360.0000
356.2500
352.5000
348.7500
345.0000
341.2500
337.5000
333.7500
330.0000
326.2500
322.5000
318.7500
315.0000
311.2500
307.5000
303.7500
300.0000
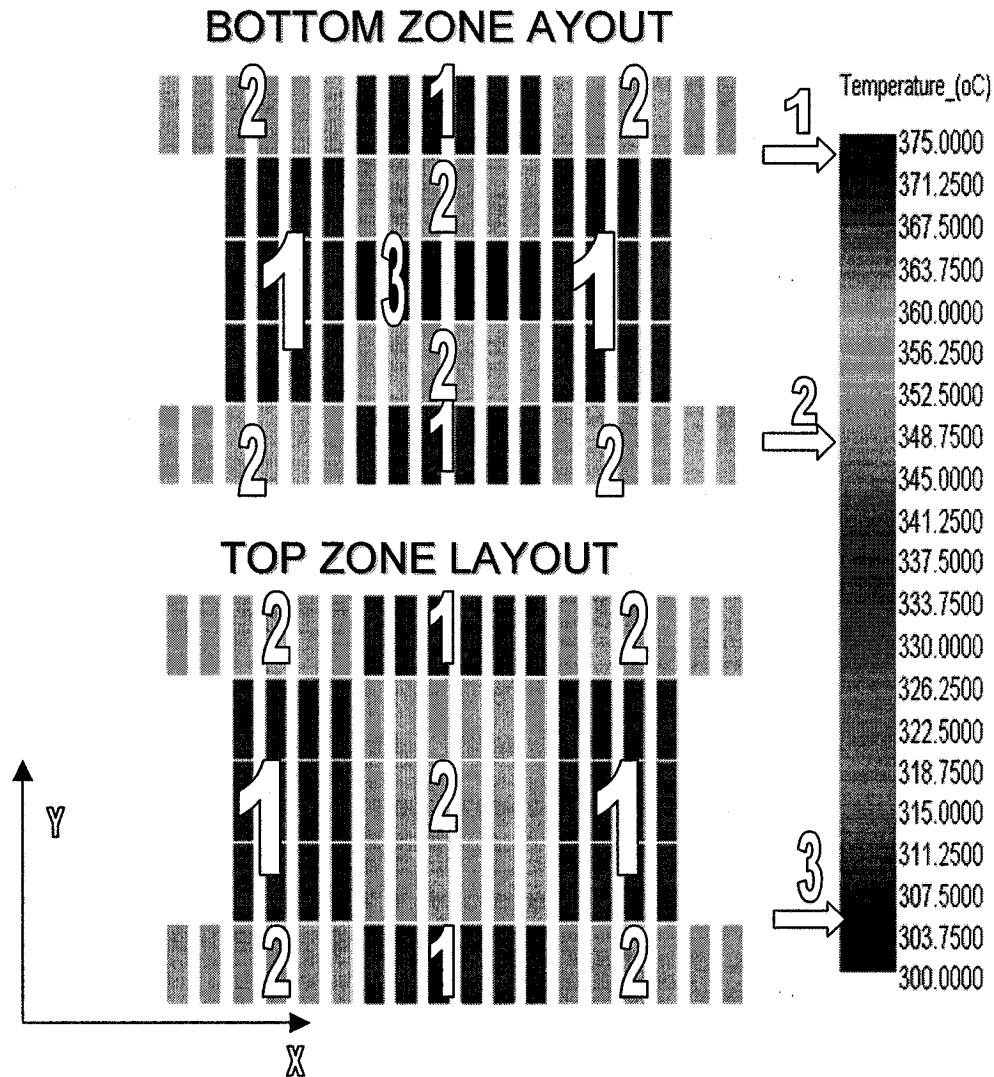
Figure 2.9: *Oven layout for Monark thermoforming machine (oven B)* *

---

* Illustration is numerated for better recognition in black and white copies.

2.3.2. Sensors

In order to perform the experimental measurements and testing, a number of sensors had to be installed on the Monark machine. These sensors were installed inside the oven and also in the forming stage and were included temperature and distance sensors. Following table details the sensor specifications installed in different sections along with their function.

Table 2.4: *Specifications of the sensors installed on Monark*

Type	Manufacturer	Model	Location	Function
Infrared temperature sensor	Raytek	RAYSHLTCF3	Inside the oven	Measuring surface temperature
Infrared line scanner	Raytek	Thermalert TF100	Exit of the oven	Recording Temperature profile along the sheet
Infrared Distance sensor	Leuze	ODS96M/V-5071-421	Bottom of the oven	Sag measurements
Infrared Distance sensor	Leuze	ODS96M/V-5110-420	Inside the plug	Measuring the bubble height

3. Characterization of Viscoelastic Properties

3.1. Introduction and Definitions

Considerable scientific and technological interest has been devoted to the understanding of viscoelastic behavior of material during the thermoforming process. In order to simulate these properties, various techniques have been used in recent years[3]. In this thesis the elastic modulus behavior with regard to temperature and frequency has been studied as a representation of the viscoelastic properties of a material.

One of the specific areas of the thermoforming process which has been more thoroughly investigated in this thesis is the transition zone between the solid and liquid state of the material. This is the area which there is presently not much available information because of the limitations of available commercial testing machines and also shortcomings in previously developed numerical models for the evaluation of the mechanical properties of materials. By applying a novel bubble inflation technique for the localized investigation of the transition zone and an elastic approach for the oven heating stage, the complete variation of the elastic modulus has been characterized on-line. This constitutes a significant advancement in this area.

A brief review of the theory of viscoelasticity and its basic principles as well as some of the available viscoelastic models is presented in the first part of this chapter. It is then followed by descriptions of applied experimental techniques for characterization of viscoelastic properties including, time-temperature superposition, the asymmetric sigmoid model and a 3D model of the elastic modulus. The last part of this chapter details

the bubble inflation technique as well as the corrected curve for the elastic modulus using the results of this experiment.

3.1.1. Theory of Viscoelasticity

The concept of the viscoelastic behavior of materials, though old in origin, has only recently come into prominence. Rheological behavior related to viscoelasticity is the most relevant for the description of a majority of real materials [27]. In general, viscoelasticity is a combination (or superposition) of properties characteristic for liquids displaying viscous dissipative losses and solids exhibiting storage of elastic energy. Therefore, a general definition of viscoelastic materials includes two components, elastic potential and intensity of dissipative losses. However, these two values are factors of different dimensions. The related characteristic material constants are viscosity and elasticity modulus. Viscoelastic behavior can be considered as a slow (or delayed) development of stresses and deformations in time, and this delay must not be confused with inertial effects also characterized by a specific lag time. This property, possessed by all plastics to some degree, dictates that while plastics have solid-like characteristics such as elasticity, strength and form stability, they also have liquid-like characteristics such as flow depending on time, temperature, rate and amount of loading.

Following is the demonstration and comparison among purely elastic, purely viscous and viscoelastic response to an applied stress. As one might notice in this figure, in the case of viscoelastic response (Figure 3.1(c)), the material's response to the applied stress is the combination of both elastic and viscous properties. The recovered part of

deformation is caused by the elastic properties of the material while the permanent deformation at the end is the direct consequence of the material's viscous properties.
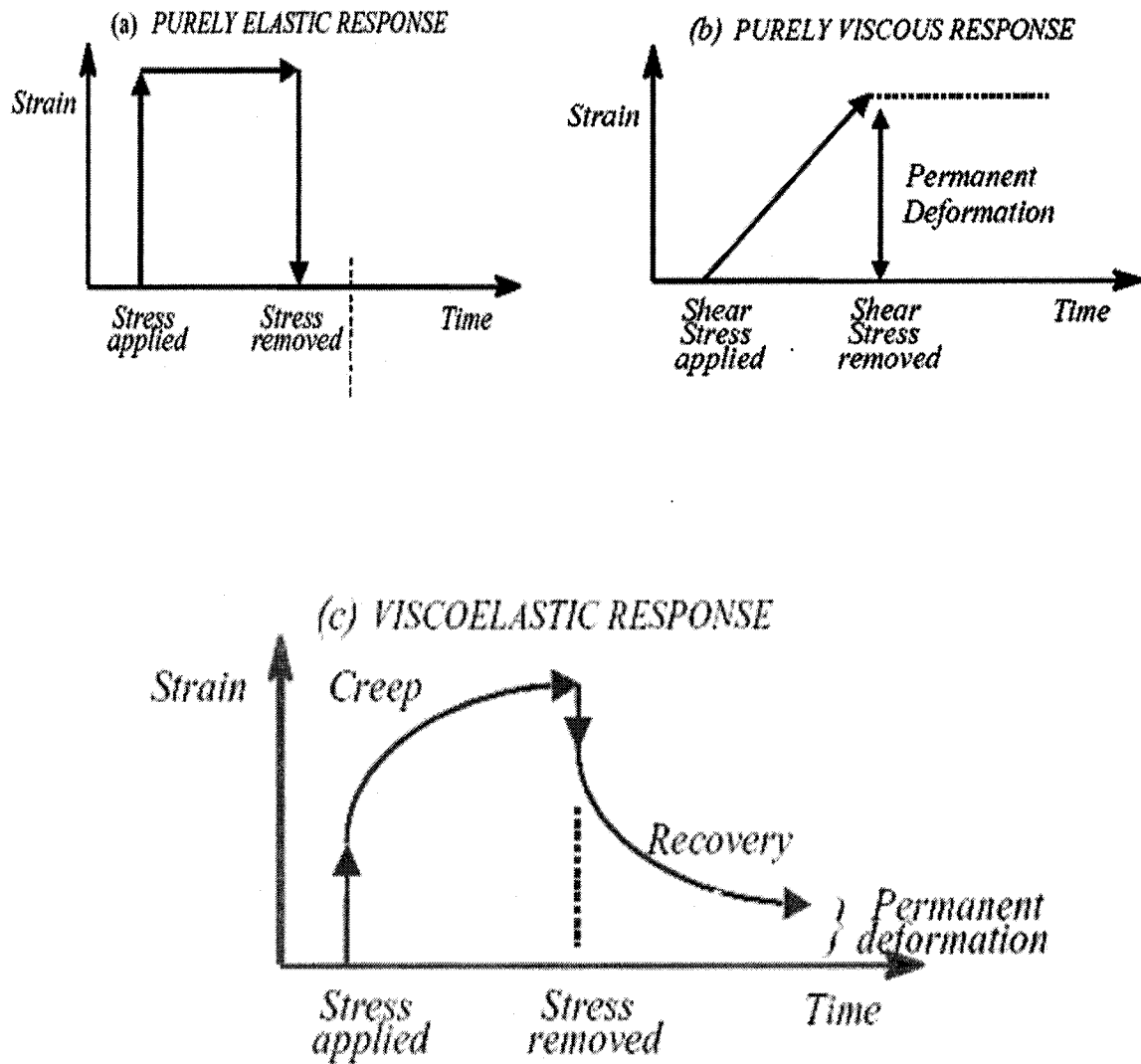
Figure 3.1: *Purely elastic, purely viscous and viscoelastic response to an applied stress.*

3.1.2. Definitions

3.1.2.1. Deborah Number

The dimensionless Deborah Number, De, was introduced as a measure of the ratio between characteristic time of observation, t_{obs}, and the time scale of inherent processes in a material, t_{inh}. Then:

Eqn. 3.1 $$De = \frac{t_{obs}}{t_{inh}}$$

The Deborah Number is especially important for viscoelastic phenomena because they always proceed over a measurable period of time. In a general sense, t_{inh} characterizes the rate of inherent rearrangement of the material structure. Since the level of structural organization, its rupture and restoration can vary, we can find very different values of characteristic times for the same material. Therefore, in principle, different values of the Deborah Number are expected to exist.

3.1.2.2. Creep

At constant stress, σ_0, applied at initial time (t = 0), slow (or delayed) development of deformations, $\varepsilon(t)$, is observed, and this phenomenon is called creep.
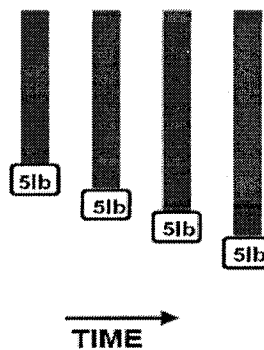
Figure 3.2: Creep: deformation under a constant load as a function of time

31
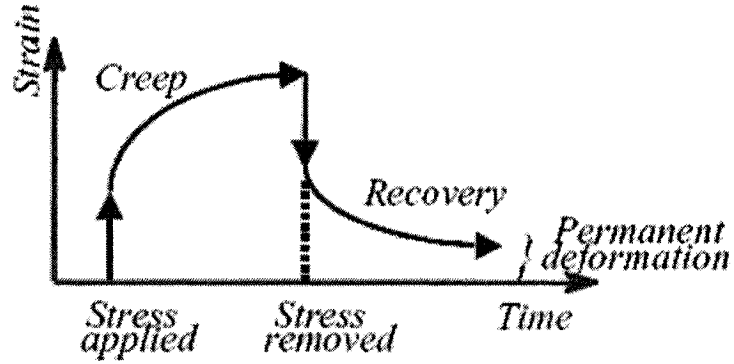
Figure 3.3: Viscoelastic response to creep

The function ε(t) can be considered as consisting of three components:

Eqn. 3.2 $\varepsilon(t)=\varepsilon_0(t,\sigma_0)+\psi(t,\sigma_0)+\dfrac{t}{\eta(\sigma_0)}\sigma_0$

where ε_0 is an instantaneous deformation, $\psi(t,\sigma_0)$ a function describing delayed development of deformations, $\eta(\sigma_0)$ viscosity, which (in a general case) can depend on stress and current time, t. Another formulation of Eqn. 3.2 is:

Eqn. 3.3 $\dfrac{\eta(t)}{\sigma}=I(t)=I_0(\sigma)+\psi(t,\sigma)+\dfrac{t}{\eta(\sigma)}\sigma$

where the value $I(t)$ is called *compliance*, I_0 an instantaneous compliance, and $\psi(t)$ is a creep function. As pointed out above, in formulating Equations 3.2 and 3.3, the type of deformation (extension, shear, and so on) is not specific, but it must be accepted that deformation is one-dimensional.

A material is called *linear viscoelastic* if material parameters, I_0, $\psi(t)$ and η, do not depend on stress; in the opposite case, material has *non-linear viscoelastic* behavior.

32

3.1.2.3. Relaxation

At constant deformation, if ε_0 is set at some initial moment of time, t=0, we can observe a slow decay of stresses in time $\sigma(t)$. This phenomenon is called relaxation. Stress relaxation is a very important phenomenon in practice. If it occurs at a slower pace than the cooling rate, some stresses may be imprisoned when the material solidifies, which can influence its quality.
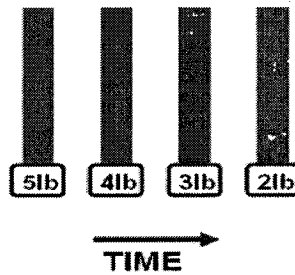
Figure 3.4: Relaxation: constant deformation experiment

Relaxation that occurs during part usage can also have an adverse effect. For example, relaxation in seals could allow gas or liquid leakages in equipment working under pressure. This can be achieved if a seal is continuously stressed during exploitation; so that relaxation leads to loss of contact between the seal and the container.

The relaxation modulus G(t) commonly serves as a characteristic material property for describing relaxation behavior. It may be directly observed in a simple experiment in which the test polymer is equilibrated first, and then, at some time t=0, it is sheared (or stretched) rapidly into a new shape where it is held while the resulting stress

can gradually relax with time. The time dependent stress, $\sigma(t)$, divided by the imposed

strain ε_0, directly gives the relaxation modulus:

Eqn. 3.4 $\qquad G(t) = \sigma(t) \big/ \varepsilon_0$

3.1.3. Viscoelastic Models

As was mentioned before, viscoelastic behavior may be linear or nonlinear.

Linear viscoelastic behavior is observed only when the deformation is very small or slow,

and therefore, it is not directly relevant to the behavior of molten polymers in processing

operations where deformations are always large and rapid. Linear viscoelastic behavior is

independent of the kinematics of the deformation and the magnitude of past strains.

These simplifications make possible the addition of the effects of successive

deformations. The Boltzman superposition principle (Eqn. 3.5) describes the linear

viscoelastic response of a material to an arbitrary strain history:

Eqn. 3.5 $\qquad \tau(t) = 2 \int\limits_{-\infty}^{t} G(t - t') D(t') dt'$

where τ is the extra stress tensor, G(t-t') is the relaxation modulus, and D(t') is the rate of

the deformation tensor at time t'.

Conversely, in a nonlinear system, the response to an imposed deformation

depends on the size, the rate and the kinematics of the deformation. Therefore, it is not

possible to measure a response from one type of deformation and use the result to predict

the response in another type of deformation, unless the rate, magnitude and kinematics of the deformation are all the same in both cases.

Two approaches have been used to formulate nonlinear viscoelastic constitutive equations. The first one is based on the derivation of molecular theories for melts and dilute solutions together with the use of statistical mechanics. This approach however does not always yield closed form constitutive models. Because of the mathematical complexity involved, many simplifying assumptions must be made, and this limits the practical value of the molecular approach.

The second method is an empirical approach based on a continuum mechanics concept. Complications in building the model arise from the involvement of tensor-valued quantities and the fact that the response of the material depends on the history of strains imposed at previous times. These complications make it difficult to establish an acceptable form of a nonlinear constitutive equation.

At the present time, there is no universal theory that describes nonlinear rheological phenomena. Nevertheless, several models have been used in numerical simulations, and these are either differential or integral constitutive equations. Some of these models which are used in this thesis are reviewed later in this study.

3.1.3.1. Mechanical Models

We can attempt to model the behavior of a viscoelastic material by combining simple mechanical elements like springs and dashpots.

Spring

In this model, stress is purely a function of the instantaneous strain. Equation 3.6 shows the relation between stress and strain for a spring mechanical model which is called *Hooke's law*. E is called the *Elastic Modulus*.

Eqn. 3.6 $\quad \sigma = E\varepsilon$

Figure 3.5: Purely elastic response represented by a spring model
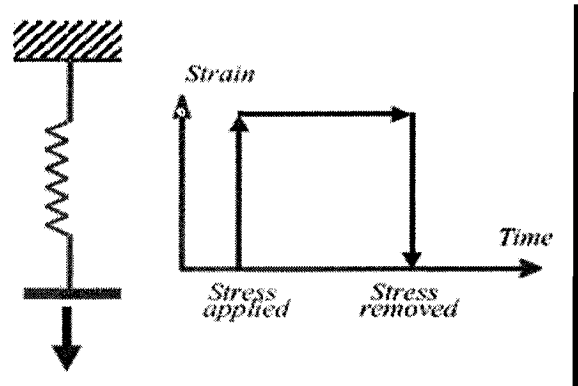
Dashpot (Damper)

In this model, strain depends on stress history, not just on stress at a moment in time.

Eqn. 3.7 $\quad \sigma = \eta \dfrac{d\varepsilon}{dt} = \eta\dot{\varepsilon}$
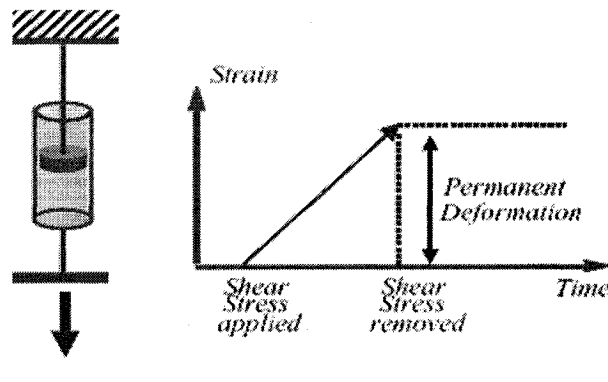
Figure 3.6: Purely viscous response represented by dashpot model

36

Maxwell Model

This model is a combination of a spring and a dashpot in series. $\sigma = \sigma_1 = \sigma_2$ and

$\varepsilon = \varepsilon_1 + \varepsilon_2$ therefore: **Eqn. 3.8** $\dot{\varepsilon} = \dfrac{\sigma}{\eta} + \dfrac{\dot{\sigma}}{E}$
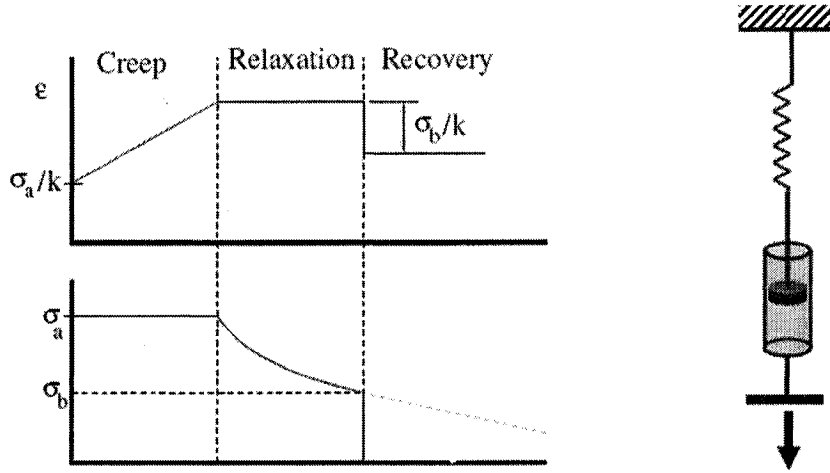
Figure 3.7: *Maxwell model and prediction of creep, relaxation and recovery periods.*

Recalling the real viscoelastic behavior (Figure 3.2), one can conclude that the Maxwell general model handles creep badly (model is without bounds at a constant rate), is also not a good model for recovery (model only recovers elastic deformation, and does so instantly), but accounts fairly well for relaxation.

In a stress relaxation experiment $\dot{\varepsilon} = 0$, because the total displacement is zero. Hence:

Eqn. 3.9 $\sigma = \sigma_0 \exp\left[\dfrac{-t}{\tau_t}\right]$ where: $\tau_t = \dfrac{\eta}{E}$

τ_t is called *relaxation time*. E(t), the elastic modulus can be deduced from this equation:

Eqn. 3.10 $E(t) = \dfrac{\sigma(t)}{\varepsilon_0} = \dfrac{\sigma_0}{\varepsilon_0} \exp\left[\dfrac{-t}{\tau_t}\right]$

37

Voigt Model

This model is a combination of a spring and a dashpot in parallel. $\sigma = \sigma_1 + \sigma_2$

and $\varepsilon = \varepsilon_1 = \varepsilon_2$ therefore:

Eqn. 3.11 $\qquad \sigma(t) = E\varepsilon(t) + \eta\dot{\varepsilon}$
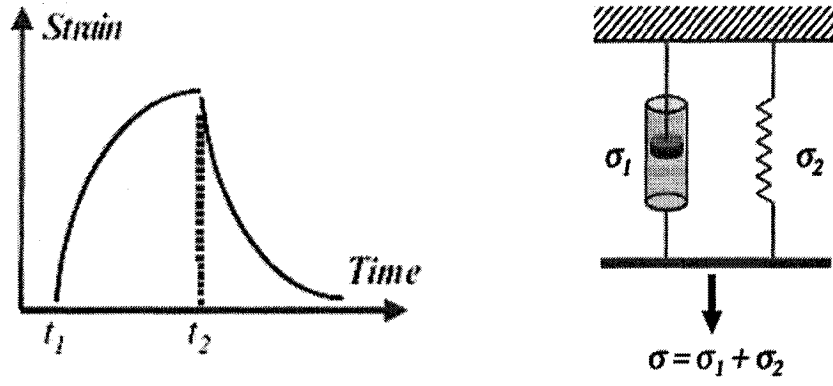
Figure 3.8: *Voigt model and retarded elastic response to a given stress.*

This model gives a retarded elastic response, but does not allow for ideal stress

relaxation, in that the model cannot be instantaneously deformed to a given strain.

However, in creep, stress is constant ($\sigma = \sigma_0$); hence,

Eqn. 3.12 $\qquad \varepsilon(t) = \dfrac{\sigma_0}{E}\left[1 - \exp\left(\dfrac{-t}{\tau_t'}\right)\right]$ where: $\tau'(t) = \dfrac{\eta}{E}$ is the *retardation time.*

Problems with simple models:

As one might notice the general Maxwell model cannot account for a delayed

elastic response, and the Voigt model does not describe stress relaxation. Both of these

models are characterized by single relaxation times; therefore, a spectrum of relaxation

times would provide a better description.

38

Different combinations of these simple models have been used by rheologists in order to describe the viscoelastic behavior of material as close as possible to experimental results. The Maxwell-Weichert model is one of these combinations of simple models which have been used in this research study.

Maxwell-Weichert Model

This model is a combination of Maxwell element in parallel (figure 3.9). The strain is the same in all the elements and the total stress is the sum of stresses in each element. Hence:

Eqn. 3.13 $\quad \dot{\varepsilon} = \dfrac{\sigma_1}{\eta_1} + \dfrac{\dot{\sigma}}{E_1} = \dfrac{\sigma_2}{\eta_2} + \dfrac{\dot{\sigma}}{E_2} = \cdots$

Considering stress relaxation: $\dot{\varepsilon} = 0$, hence:

Eqn. 3.14 $\quad \sigma_1 = \sigma_0 \exp\left[\dfrac{-t}{\tau_{t1}}\right], \ \sigma_2 = \sigma_0 \exp\left[\dfrac{-t}{\tau_{t2}}\right], \ \ldots\ldots$
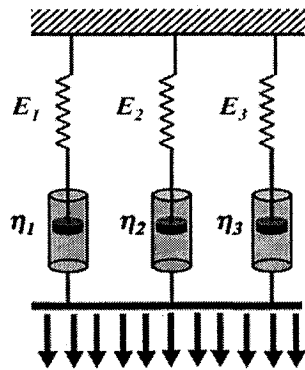
Figure 3.9: Maxwell-Weichert Model

39

Including $\sigma = \sigma_1 + \sigma_2 + \cdots$ and equations 3.13 and 3.14 gives equation 3.15:

Eqn. 3.15 $E(t) = \sum_{i=1}^{n} E_i \exp\left(\frac{-t}{\tau_{ti}}\right)$

where: $E_i = \dfrac{\sigma_{0i}}{\varepsilon_0}$ and n is the number of Maxwell elements in parallel and τ_{ti} is the

relaxation time.

3.1.3.2. Numerical Approaches

The solution of viscoelastic modeling problems presents several numerical challenges in the case of both differential and integral constitutive models. However, certain similarities exist between the two cases, for example, the nonlinear character of the governing equations brought about by the constitutive equation for the viscoelastic stresses. Many discretization techniques have been used to solve the conservation and constitutive equations, and these include finite elements, boundary elements, finite difference and spectral methods. The majority of published simulations have been carried out using finite element methods for both differential and integral constitutive equations. This is due to the advantages of finite element methods in discretizing arbitrary geometries and imposing simply and accurately a variety of complex boundary conditions.

3.2. Time-Temperature Superposition

The idea of superposition based on the influence of different factors on viscoelastic properties is widely used to model the behavior of viscoelastic materials. In this part of chapter three, this method is explained in detail and applied to the prediction

of the elastic modulus at a given temperature. A master curve is thus prepared. This master curve is then characterized for the specific material. The advantages and disadvantages of this method are then discussed.

3.2.1. General Approach

This approach can be formulated in the following way: the same value of any viscoelastic function can be obtained *either* by changing the time (frequency) *or* the physical state of material; the latter is governed by changes in process parameters such as temperature, concentration of components, or other parameters. Sometimes, it can be a very unexpected parameter; for example, it can be a duration of exposure of a material to ultraviolet radiation of the Sun (important for predicting long-term behavior of organic glasses in illuminators of air-liners). The superposition principle is illustrated in Figure 3.10.

Consider two experimental points for an imaginary viscoelastic function $\alpha(t)$, measured on the same time base, t_1, but at two different temperatures, T_1 and T_2.

The value of the function at α_2 can be obtained in two ways; first, as shown in Figure 3.10, by direct measurement at temperature T_2 during time t_1, and second, at temperature T_1, but with time base t_2. If we can find a coefficient a_T which characterizes the temperature dependence of this function, we can *shift* the point (t_1, α_1) to the position (t_2, α_2) as shown by the arrow in Figure 3.10.
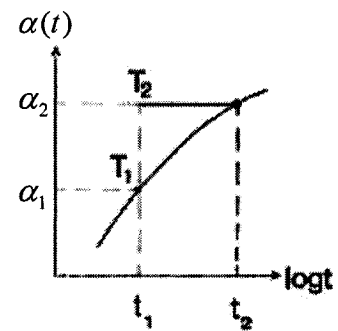
Figure 3.10: Idea of Superposition

41

The temperature coefficient a_T is calculated as:

Eqn. 3.16 $a_T = \log \dfrac{t_2}{t_1}$

or in general form:

Eqn. 3.17 $a_T = t^* a_T(T)$

where t^* is a constant and $a_T(T)$ is a function characterizing the temperature dependence of viscoelastic properties. A very important hypothesis is that this function is the same for any viscoelastic function. This can be proven by the existence of mutual interrelations between different functions characterizing the viscoelastic behavior of materials.

Now, after shifting the point on the function $\alpha(t)$, (t_1, α_1) into a new position (t_2, α_2), we have obtained two points on the isothermal (at T_1) curve and we can try to reconstruct the function curve as shown in Figure 3.10. In fact, by superposing the results of the measurements of the viscoelastic functions on the limited time (frequency) base or "window" (in Figure 3.10, it is only one point at t_1), one has a possibility to extend the range of experimental determination of this function.

It is a very important method because in real experimental practice, we rarely have a chance to make measurements beyond the range of $1\text{-}10^4$ s or $10^2\text{-}10^3$ Hz, except by using the method of superposition. We can extend this range practically without limit and cover the range of 12-15 decimal orders in time or frequency.

However in many real situations, we do not know the temperature coefficient, $a_T(T)$, beforehand. In order to obtain its value, it is not sufficient to measure only one point for every temperature. It is necessary to obtain a relationship with some

42

points having the same values of a viscoelastic function. This approach is illustrated in Figure 3.11.

We have two sections of the E(t) dependencies measured at two temperatures. In this case, the temperature coefficient is found as a distance between two curves where the values of the modulus at the two temperatures appear to be the same, E_0. The reduced time-scale is calculated as $t/a_{(T)}$.
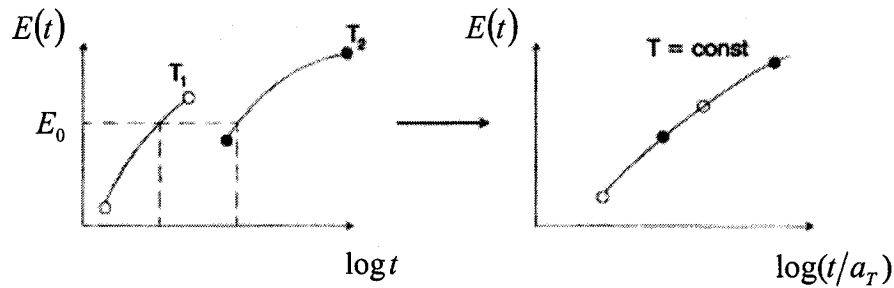
Figure 3.11: Superposition of two portions of the time dependencies of the elastic modulus measured at two temperatures.

It is possible to find hundreds of examples of applications of the time-temperature superposition in publications devoted to measuring properties of polymeric materials. In order to illustrate the power of this method we shall discuss one conditional (but close to reality) example of superposition of the elastic modulus measured over a rather limited time range (Figure 3.12). The experimental "window" is no wider than 3 decimal orders, and therefore, only very limited portions of the full E(t) dependence are known. Superposition opens this window and we can now know the values of this dependence over a very wide range of time (or frequencies).

43
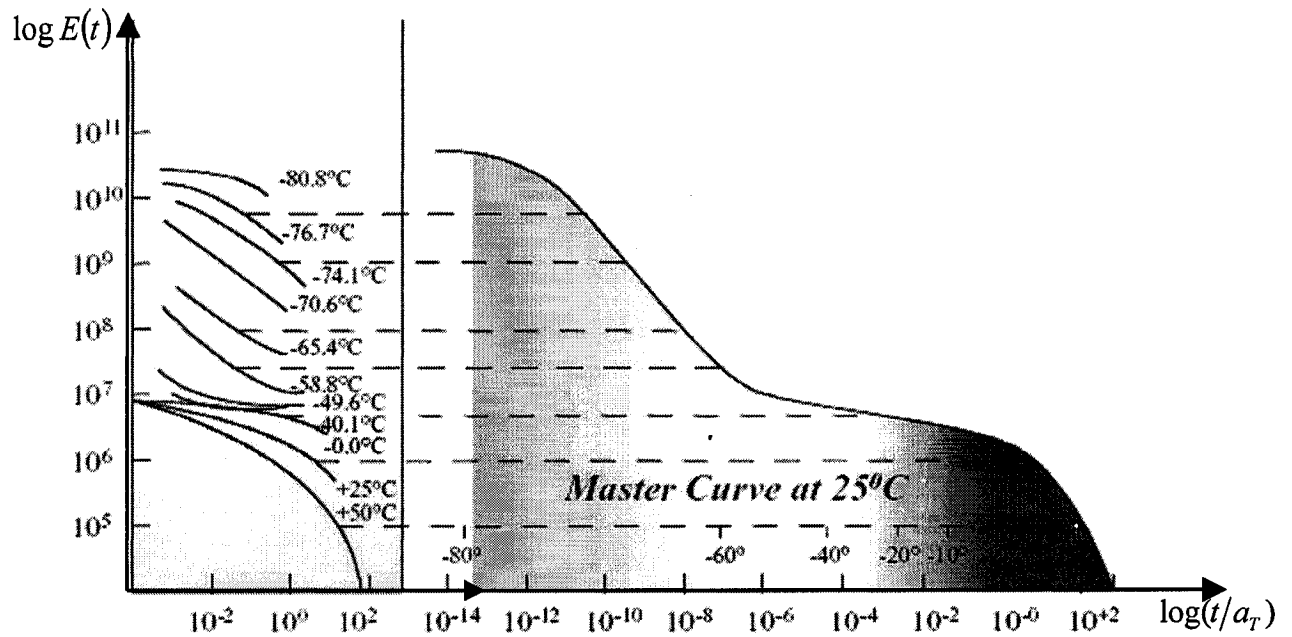
Figure 3.12: Example illustrating superposition of many portions of time dependencies of elastic modulus measured at different temperatures

An empirical approach to time-temperature superposition is possible if all neighboring portions of the curve have common points. We do not need to know the $a_T(T)$ function. However, such treatment of data is not always possible, and in many cases, not even convenient. That is why it is important to know the $a_T(T)$ function beforehand.

It was proven experimentally that two possible expressions have general meaning for the $a_T(T)$ function. The first of them is the *Arrhenius-Eyring* exponential equation, proposed as an analogue to the kinetic equation for the rates of chemical reactions.

Eqn. 3.18 $\qquad a_T = Ae^{E/RT}$

44

where A is a front-factor (coefficient) and E is the energy of activation of relaxation processes. If we choose some temperature T_o, as a *reference point* (i.e., if we reduce all experimental data to this selected temperature), then the Arrhenius-Eyring equation can be written as:

Eqn. 3.19 $$a_T = \exp\left[\frac{E}{R}\left(\frac{1}{T} - \frac{1}{T_0}\right)\right]$$

The second expression for the $a_T(T)$ function, which is widely used for time-temperature superposition of experimental data in various polymeric materials (it must be emphasized that polymeric materials and polymer-based compositions are the main object for application of superpositions of different types), is the so-called *Williams-Landel-Ferry (WLF)* equation, which can be written as:

Eqn. 3.20 $$\log a_T = \frac{-c_1(T - T_{ref})}{c_{2+}(T - T_{ref})}$$

where T_{ref} is the reference temperature, and c_1 and c_2 are constants depending on the choice of the reference temperature.

If the glass transition temperature is assumed as a reference temperature, the values of these constants appear rather stable. In fact it is a rough approximation, and it is preferable to use individual values of the constants, which are different for various materials. As a general rule, it is thought that the Williams-Landel-Ferry equation is true in the temperature range from the glass transition temperature, T_g, up to $T_g + 100°C$. The Arrhenius-Eyring equation can successfully be used in the range of temperatures approximately at $T > T_g + 100°C$.

If we know the form of temperature dependence of a_T, it allows us not to have to measure the function $a_T(T)$ in the whole range of temperatures, but to restrict measurements to a few points in order to verify the constants entering these equations.

The method of superposition is not limited to the reduction of data by changing the temperature only. The state of a material can be changed for different reasons. For example variations in content (concentration) of a polymer in a solution are often used to change its relaxation properties. From this we can realize time-concentration superposition, and so on.

3.2.2. Experimental Results

Material Definition

Table 3.1 shows the material type and grade used in this experiment.

Table 3.1: Material definition

Type	Grade	Trade Name	Manufacturer
HDPE	DMDF 6200	HDPE 6200	Petromont

Experimental Data

In this experiment the data is given as a table of elastic modulus (Young's modulus) versus time for a number of temperatures (typically 6 to 8). This data was extracted out of the provided DMA (Dynamic Mechanical test Analysis) test results done by Petromont Inc.

The first step in applying the time-temperature superposition technique is to

generate all the curves related to different temperatures at the given times (Figure 3.13).
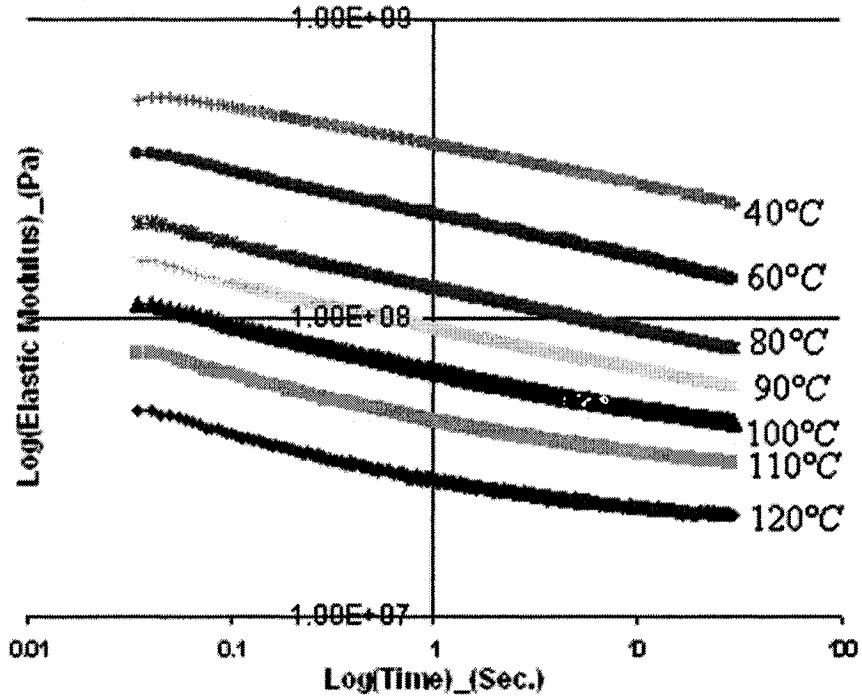
Figure 3.13: *Time dependencies of elastic modulus measured at different temperatures*

As was explained in section 3.2.1, the next step is to shift the curves with regard to the

reference temperature (T_{ref} being given by the user, depending on the nature of the

material; here, we chose T_{ref} =40°C.) in order to find the shift factor $a_T(T)$.(Figure 3.14)
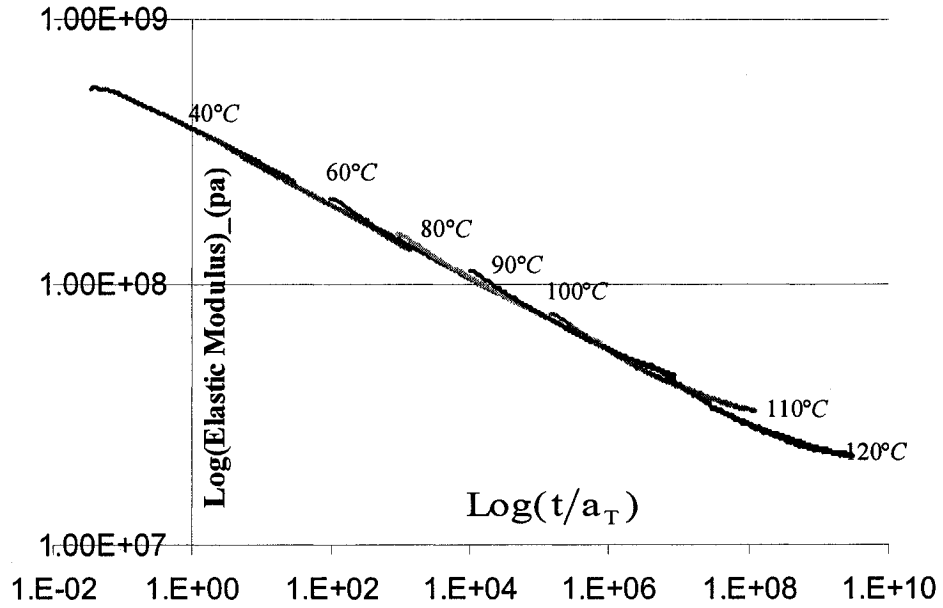
Figure 3.14: *Generation of the master curve (time-temperature superposition)*

Now we can find the WLF coefficients C_1 and C_2 by using a linear fit technique.

Table 3.2 shows the shift factor at different temperatures.

Table 3.2: *Calculating WLF coefficients using the linear fit technique*

Temp.(°C)	a_T	$T-T_{ref}$	$log(a_T)$	$-\dfrac{T-T_{ref}}{Log(a_T)}$
40	1	0	0	
60	0.022	20	-1.6576	12.0658
80	0.00037	40	-3.4318	11.6557
90	0.00004	50	-4.3979	11.369
100	0.0000036	60	-5.4437	11.0219
110	0.00000025	70	-6.6021	10.6028
120	0.00000001	80	-8	10

Equation 3.21 can be derived from the WLF equation (Eqn. 3.20):

Eqn. 3.21
$$-\frac{T-T_{ref}}{Log(a_T)} = (T-T_{ref})\left(\frac{1}{c_1}\right)+\left(\frac{c_2}{c_1}\right)$$

48

By comparison to the general linear equation y=ax+b, by plotting $-\dfrac{T-T_{ref}}{Log(a_T)}$

versus $\left(T-T_{ref}\right)$, and by finding the linear fit, the WLF coefficients are found. See C_1 and C_2 in Figure 3.15.
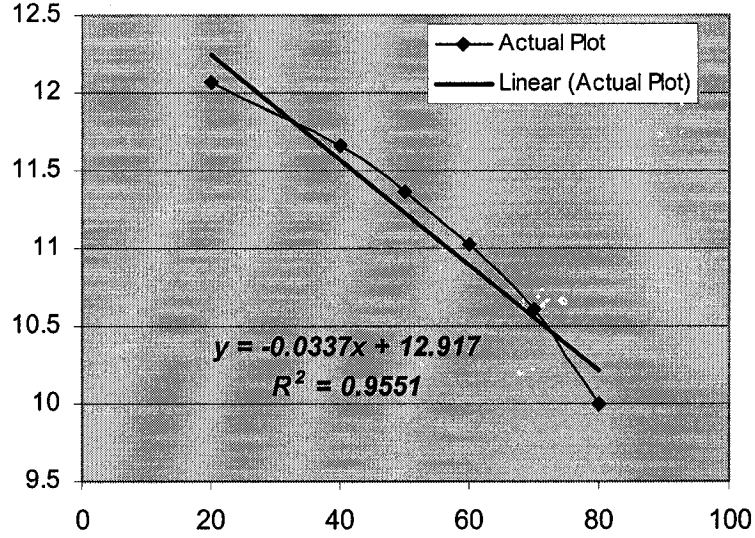
Figure 3.15: *Finding WLF coefficients by applying linear curve fitting*

Hence, $C_1 = -29.67$ and $C_2 = -383.3$.

As a result, a master curve has been determined by applying the time-temperature superposition technique.

3.2.3. Characterization

The stated goal is to characterize the generated master curve for the elastic modulus by applying a viscoelastic model. After considering different models, it was concluded that the Maxwell_Weichert model (explained in section 3.1.2.1) with six elements, is the best fit for the generated curve.

Recalling the general equation for this model:

Eqn. 3.22
$$E(t) = \sum_{i=1}^{n} E_i \exp\left(\frac{-t}{\tau_{ti}}\right) \quad \text{where:} \quad E_i = \frac{\sigma_{0i}}{\varepsilon_0}$$

In this equation, **n** is the number of relaxation times (number of Maxwell elements in parallel) requested by the user (6 in this case), τ_{ti} are the relaxation times and E_i are the elastic moduli. The fitted master curve is normalized by:

Eqn. 3.23
$$G(t) = \frac{E(t)}{E_0} = \sum_{i=1}^{n} g_i Exp\left(\frac{-t}{\tau_{ti}}\right)$$

where: $g_i = \frac{E_i}{E_0}$; $\sum_{i=1}^{n} g_i = 1$ and $E_0 = \sum_{i=1}^{n} E_i$.

Table 3.3 shows the calculated values for six relaxation times and elastic moduli using the solver function in Microsoft® Excel.

Table 3.3: *Maxwell-Weichert model parameters*

i	1	2	3	4	5	6
E_i	173.0066	135.0003	87.13369	54.90298	33.3159	29.378
τ_{ti}	0.835562	2.17E+01	6.88E+02	5.30E+04	1.00E+07	1.00E+10
g_i	0.337417	0.263293	0.169938	0.107078	0.064977	0.057296

$E_0 = 512.737$ MPa

Figure 3.16 illustrates the Maxwell-Weichert fit with 6 relaxation times.
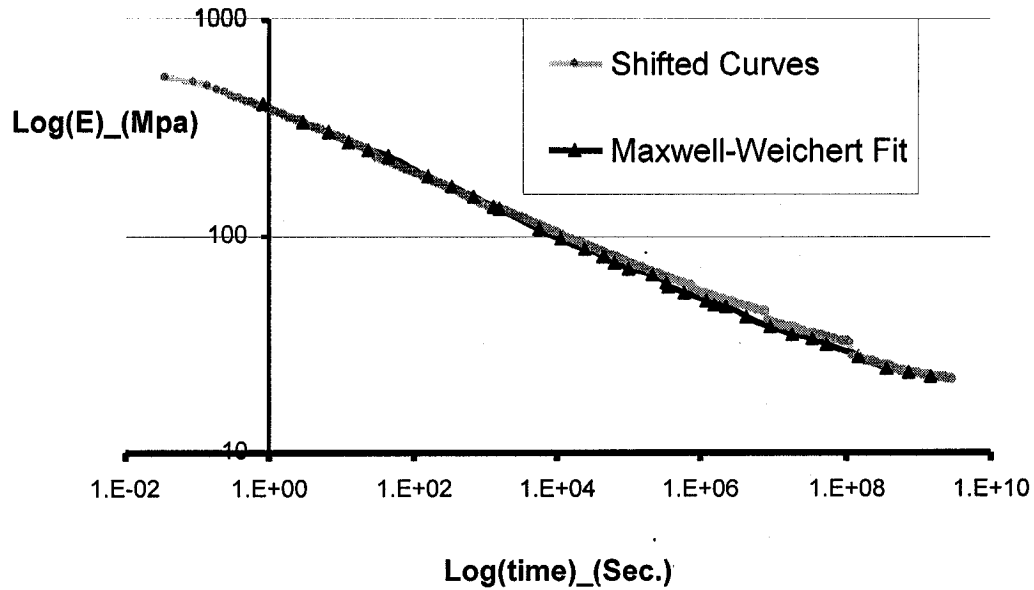
Figure 3.16: Time-temperature superposition plot and the Maxwell-Weichert fit

3.2.4. Conclusions

> The method of superposition, used to reduce the experimental data along the time (frequency) scale, greatly increases the range of the fit.

> At the same time, it must be remembered that the *main principle* of the method is based on the assumption that in changing the state of a material, its relaxation spectrum changes in the same manner for *all* relaxation times, i.e., no new relaxation process appears, no process disappears, and temperature dependencies of all relaxation times in a spectrum are the same.

➢ This assumption is confirmed by the fact that the temperature dependence of any relaxation time is the same as the viscosity, and we know that viscosity is the integral representation of all relaxation times. At the same time, it is a rather strong assumption which may not be fulfilled, especially if superposition is carried out for initial experimental data obtained in a wide temperature range. In fact, many cases are known in which this basic assumption is wrong. One of the most evident examples is a phase transition. If it takes place in the temperature range under discussion, it definitely leads to radical changes in relaxation properties. The danger is rather serious for crystalline and semi-crystalline polymers because their crystallization process takes place in a wide temperature range.

➢ Time-temperature superposition is not a universal method and has definite limitations. That is why one must be very careful when treating experimental data by this method, especially if extrapolation beyond the experimental window, is attempted.

➢ In this specific study which characterizes the viscoelastic properties in the thermoforming process, we are dealing with a wide range of temperatures which includes phase changes in the polymer. Therefore, notwithstanding the fact that this technique predicts the initial part of the material's behavior in a perfect

manner, overall it is not the best method to be applied to the whole thermoforming process.

> A method which would cover the whole temperature change during the thermoforming process is needed, and this will be presented in the following chapters.

3.3. Asymmetric Sigmoid Model for Elastic Modulus

3.3.1. Experimental Results

Material Definition

The following tables show the material definition and properties for HDPE.

Table 3.4: Material Definition and properties (HDPE BA50-100)

Type	HDPE (High Density Polyethylene)
Grade	BA50-100
Manufacturer	ExxonMobil Chemical
Description	High molecular weight, high density polyethylene copolymer with superior stress crack resistance, high impact strength and good rigidity
Applications	Recreational thermoformed part Large Part Blow Molding Automotive fuel tanks (monolayer) Heavy gauge sheet, typically 0.050 in to 0.500 in Automotive dunnage pallets

Resin Properties	Test Based on	Units SI (English)	Typical Values[1]
Melt Index, 190/2.16	ASTM D-1238	g/10 min	<0.1
Flow Rate, 190/21.6 (HLMI)	ASTM D-1238	g/10 min	10
Density	ASTM D-4883	g/cm^3 (lbs/ft^3)	0.949 (59.3)

Molded Properties[2]

Mechanical (23°C, 50% relative humidity, unless otherwise noted)

Tensile Strength at Yield	ASTM D-638	MPa (psi)	26 (3,800)
Elongation at Break	ASTM D-638	%	1,000
Flexural Modulus[3]	ASTM D-790	MPa (psi)	1,240 (180,000)
Tensile Impact	ASTM D-1822	joules/cm^2 (ft lbs/in^2)	25 (120)
Tensile Impact @ -40°C	ASTM D-1822	joules/cm^2 (ft lbs/in^2)	21 (100)
Impact Brittleness Temperature	ASTM D-746	°C (°F)	<-76 (<-105)
Environmental Stress Crack Resistance[4]	ASTM D-1693	hrs	>800

Thermal

Vicat Softening Temperature	ASTM D-1525	°C (°F)	120 (250)
Heat Deflection Temperature, 66 psi	ASTM D-648	°C (°F)	70 (160)
Coefficient of Linear Thermal Expansion	ASTM D-696	cm/cm/°C (in/in/°F)	1.2×10^{-4} (7×10^{-5})

Experimental Data

In this experiment the data was provided by IMI rheological laboratories and was given as a table of the real and imaginary parts of the elastic modulus, E' and E'', for a number of temperatures at different frequencies. Table A.1 in the appendix section presents the complete experimental data.

The data in the solid state was extracted by the DMTA (Dynamic Mechanical Test Analysis) technique and in the molten state by the RMS (Rheological Mechanical Spectrometer) technique. Figure 3.17 illustrates the curves generated for different frequencies. The goal is to model the curves using the minimum number of parameters.

E' and E" versus Temperature
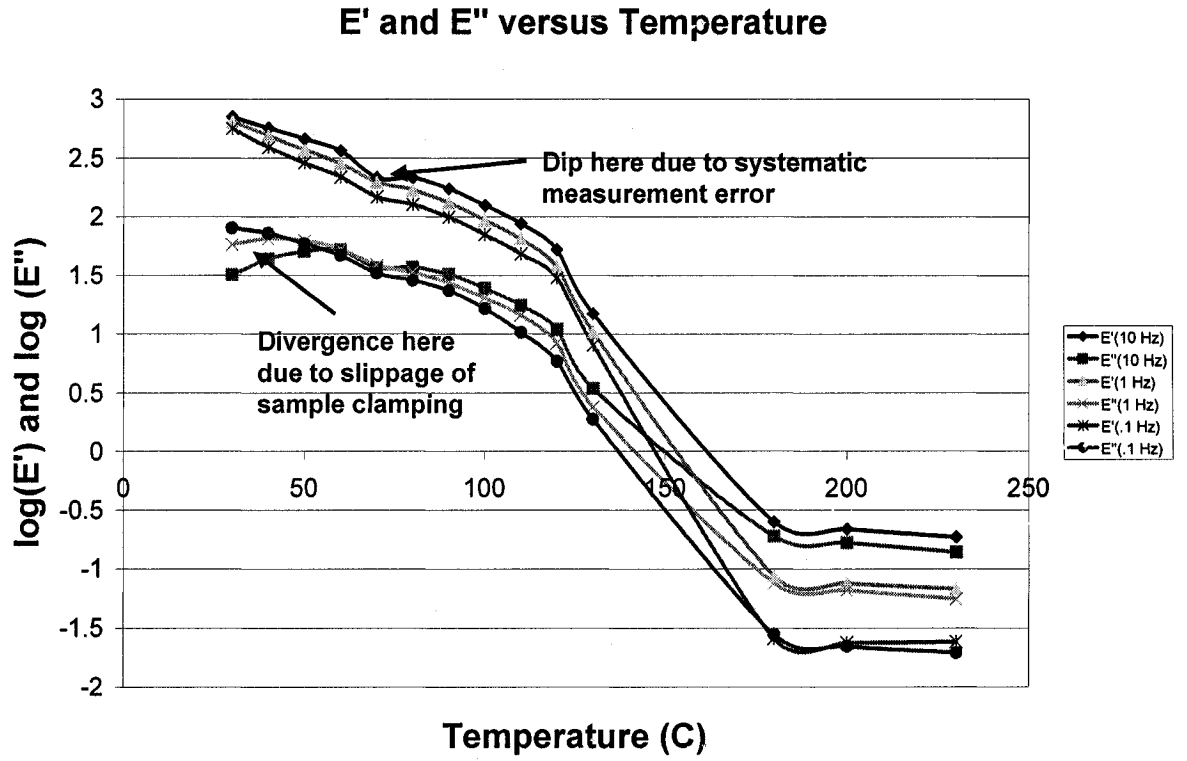
Figure 3.17: *Experimentally generated curves for E' and E'' at different frequencies*

3.3.2. Identification of parameters

In this model, the generated curve for the elastic modulus at one frequency was fit by an asymmetric sigmoid curve, and then, the shift factors for other frequencies were calculated. The general equation for the asymmetric sigmoid is:

Eqn. 3.24
$$E' = a_0 + \frac{a_1}{\left(1 + \exp\left(-\dfrac{T - a_3 \ln\left(2^{1/a_4} - 1\right) - a_2}{a_3}\right)\right)^{a_4}}$$

where a_0 to a_4 are the five parameters of this equation and T stands for temperature. These parameters are verified using "Table curve 2D", an advanced graphical software. Table 3.5 shows the values of the fitted parameters for E' and E'' at different frequencies.

Table 3.5: Parameters for the asymmetric sigmoid fit at different frequencies

	a_0	a_1	a_2	a_3	a_4
E' 10 Hz	2.985945	-3.68731	133.9327	7.744012	0.159721
E' 1 Hz	2.988273	-4.13755	135.5464	5.700672	0.109765
E' 0.1 Hz	2.986351	-4.60627	139.561	0.649299	0.011127
E" 10 Hz	1.902168	-2.7204	132.581	10.83217	0.324093
E" 1 Hz	1.942945	-3.16557	132.9732	10.40245	0.292153
E" 0.1 Hz	2.028863	-3.71769	134.4969	9.478457	0.220667

Figures 3.18 and 3.19 illustrate the experimental and asymmetric sigmoid fit curves for E' and E''. The black curves are the experimental ones and the grey curves are the fits. Obviously the fit is so close that the two curves are barely distinguishable.

Now in order to have a master curve from which all the other curves can be deduced, we have to set a frequency for E' and E'' as the reference frequency and calculate the shift factors for the other frequencies. In this analysis we assumed 10 HZ as our reference frequency. Also, in order to find the shift factors for other frequencies with minimum error, the temperature range was divided into two segments. The first range is from 30 to 130°C and the second is from 180 to 230 °C. Table 3.6 shows the shift factors for two different ranges.
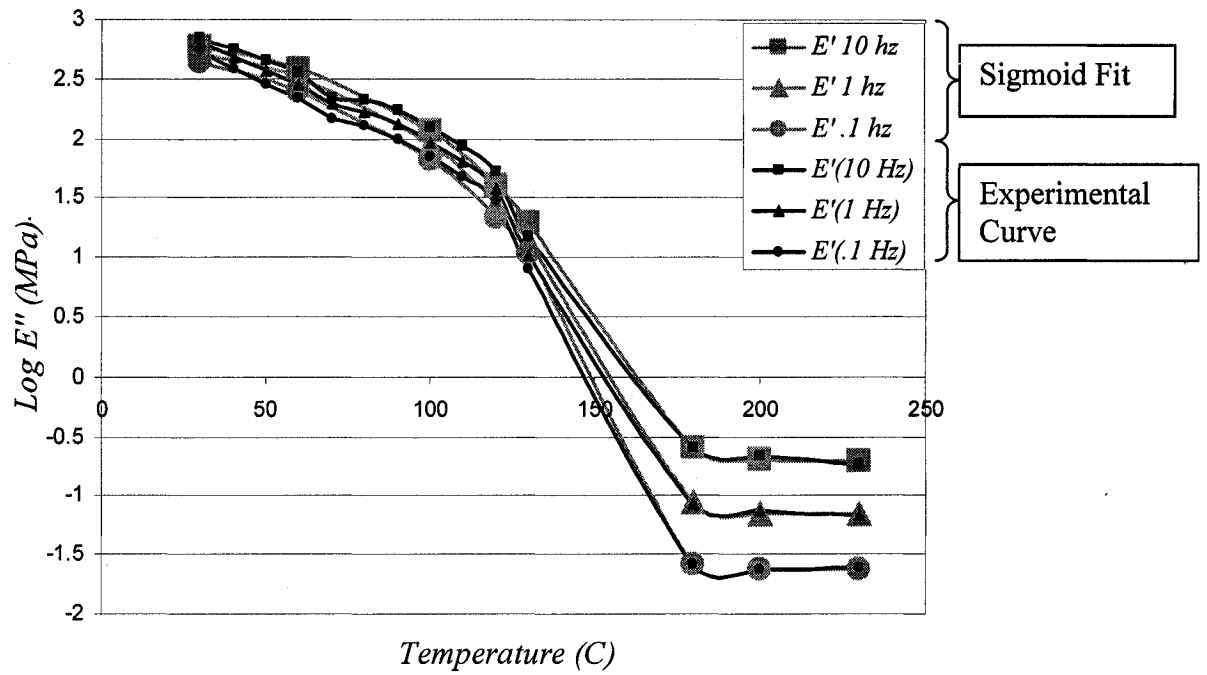
Figure 3.18 *Experimental graphs for E' along with the asymmetric sigmoid fits*
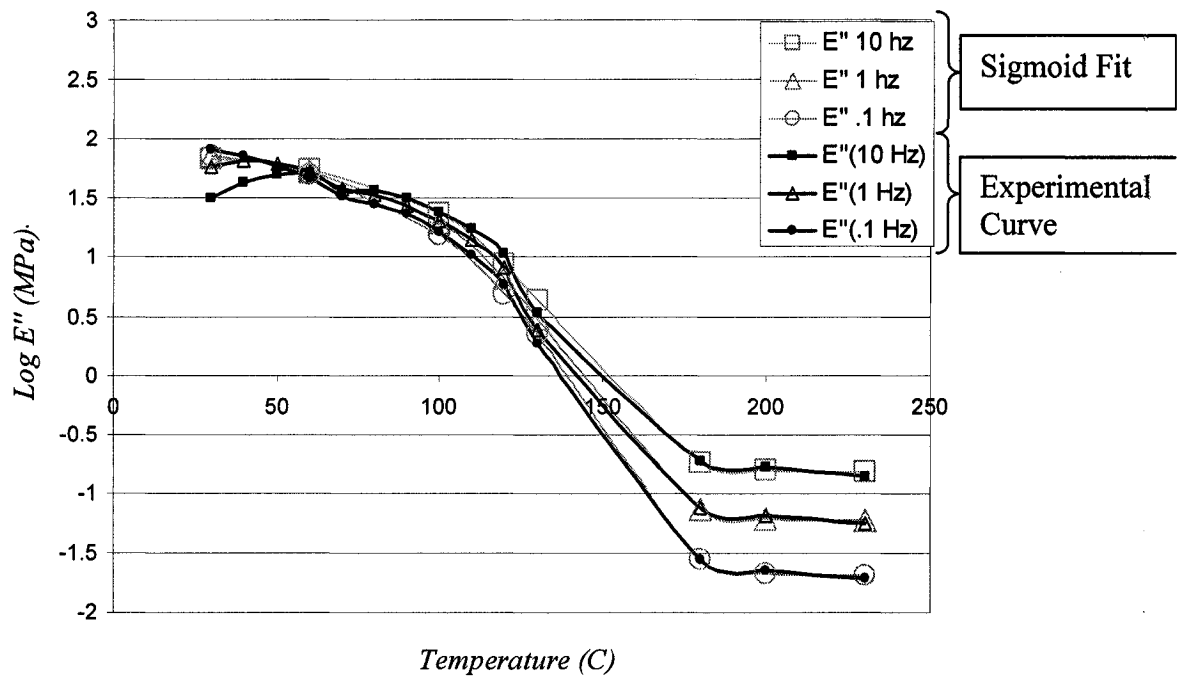
Figure 3.19 *Experimental graphs for E" along with the asymmetric sigmoid fits*

Table 3.6: *Frequency shift factors for E' and E"*

Freq. Shift Factors 30-130 Y=AX+B		
	A	**B**
E' 1Hz Γ E' 10Hz	-0.0009	1.021
E' .1Hz Γ E' 10Hz	-0.0014	1.0068
E" 1Hz / E" 10Hz	-0.002	1.1069
E".1Hz / E" 10Hz	-0.0038	1.1908
Freq. Shift Factors 180-230 Y=AX+B		
	A	**B**
E' 1Hz Γ E' 10Hz	-0.0025	2.1961
E' .1Hz Γ E' 10Hz	-0.0064	3.7403
E" 1Hz / E" 10Hz	-0.0006	1.6356
E".1Hz / E" 10Hz	-0.0007	2.2151

Figure 3.20 demonstrates the two master curves for the real and imaginary part of the elastic modulus at the reference frequency.
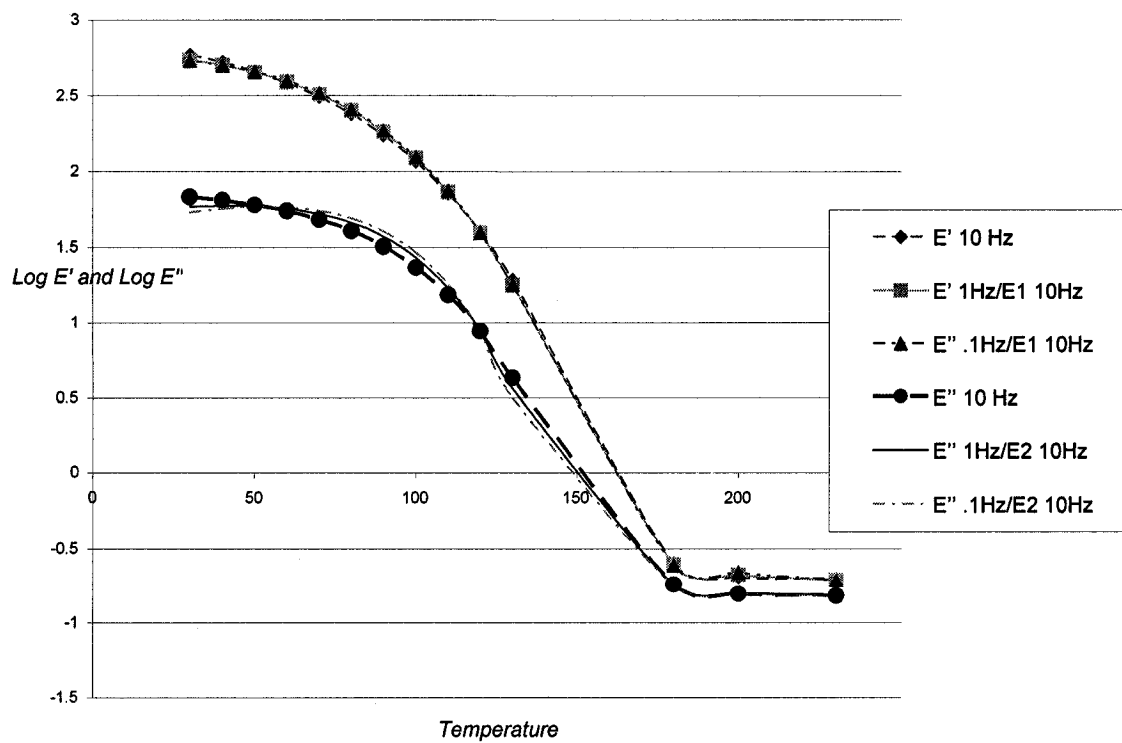
Figure 3.20: *Master curves at the reference frequencies for E' and E"*

The last step is to shift the master curve for E'' to fit the master curve for E', and to calculate the shift factors for the two ranges. Table 3.7 shows the related shift factors.

Table 3.7: Shift factors for fitting the two master curves for E' and E'

Shift Factor E" to E' Y=CX+D		
	C	**D**
From 30-130	-0.0006	0.7012
From 180-230	-0.0014	1.4671

3.3.3. Conclusions with respect to asymmetric sigmoid model for elastic modulus

➤ By applying the asymmetric sigmoid simulation technique a master curve was successfully generated for HDPE BA5-100. The two parts of the elastic modulus E'' and E' were fitted for the whole temperature range.

➤ A total of nine parameters were required for an adequate fit: five parameters for the asymmetric sigmoid equation, two for the frequency shift factor and two for extracting the imaginary part (E'').

➤ One of the areas that should be improved is the reduction of the number of dependent parameters in order to simplify the identification procedure.

➢ The main drawback of the asymmetric sigmoid simulation technique is the temperature range separation which makes the simulation procedure more complex.

➢ In the next section, these drawbacks are addressed by applying a 3D simulation technique.

3.4. Three Dimensional Simulation of Elastic Modulus

As was explained previously, the main drawback of the asymmetric sigmoid simulation technique was the treatment of the data into two temperature ranges in order to find the shift factors for the other frequencies. Another issue was to reduce the number of parameters. To this end, a three dimensional simulation software called "Table curve 3D" was used in order to characterize the generated 3D surface.

3.4.1. Modeling and characterization

Using the same experimental data (Table: A.1) as used for the previous method, a three dimensional surface is generated. Figure 3.21 illustrates the generated surface fit based on the experimental data points which are shown as diamonds.
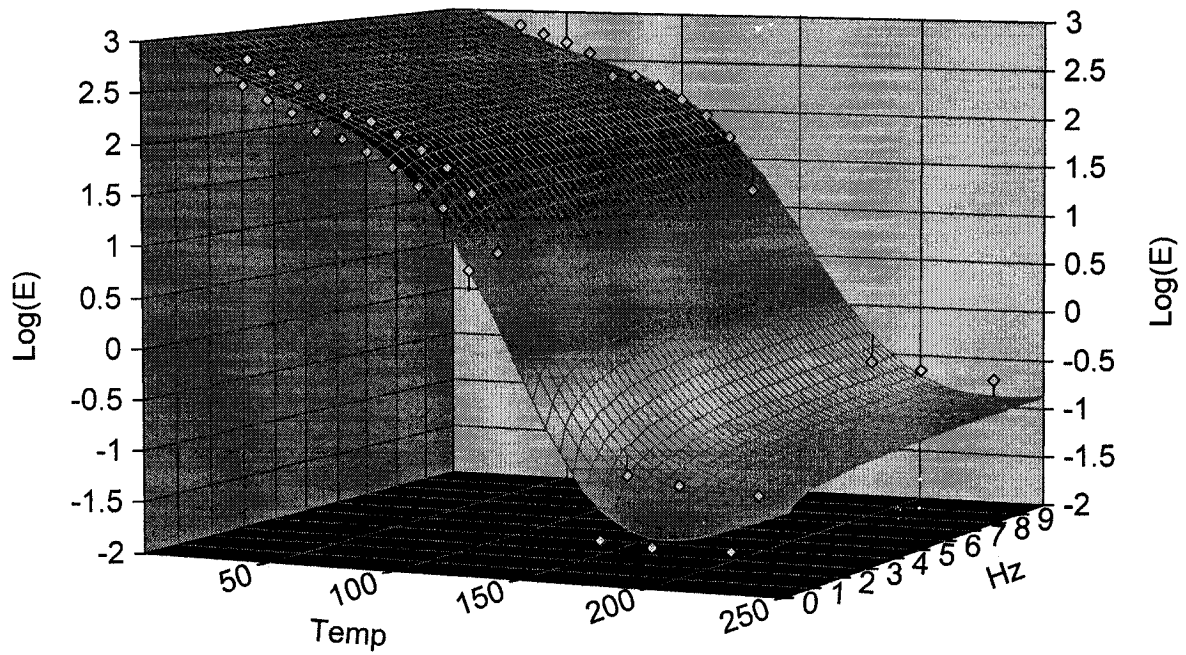
Figure 3.21: *3D simulation of elastic modulus versus frequency and temperature*

This fit was chosen after considering many factors in comparison with the other generated fits. The main advantage of this fit is its accuracy with a correlation coefficient of more than *99%* with only seven parameters. Equation 3.25 shows the fitted equation.

Eqn. 3.25
$$LogE = \frac{a_0 + a_1 T + a_2 \ln \lambda}{1 + a_3 T + a_4 T^2 + a_5 T^3 + a_6 \ln \lambda}$$

where E is the elastic modulus (it could be either E' or E'') in MPa, T is temperature in °C, and λ is the frequency in Hz. Table 3.7 shows the calculated parameters for E'.

61

Table 3.8: *Parameters for E', 3D fit equation*

a_0	a_1	a_2	a_3	a_4	a_5	a_6
3.218215	-0.02059	0.119979	0.000281	-8.2E-05	3.73E-07	0.040367

Below is a demonstration of the simulated curves by applying Eqn. 3.25 for three frequencies compared to the experimental graphs.
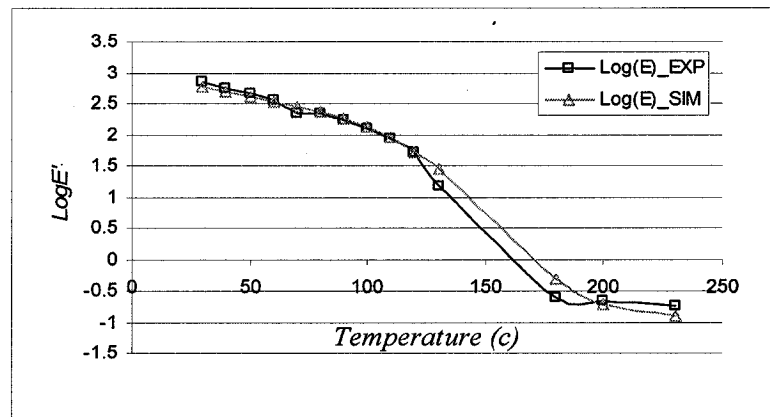
Figure: 3.22 *E' simulated and experimental curves at 10 HZ*
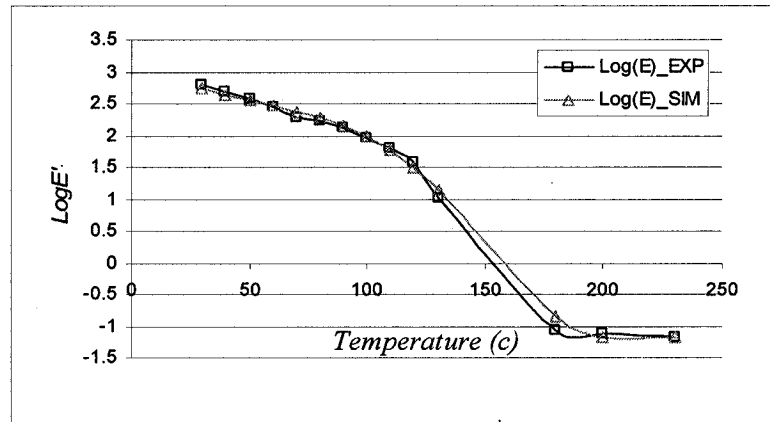
Figure: 3.23 *E' simulated and experimental curves at 1 HZ*
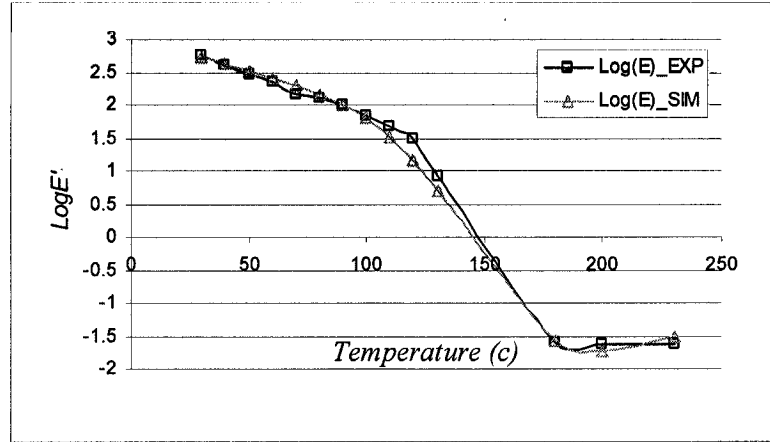
Figure: 3.24 *E′ simulated and experimental curves at 0.1 HZ*

3.4.2. Conclusions with respect to three dimensional simulation of elastic modulus

➤ By applying the three dimensional simulation technique, it is possible to predict the elastic modulus of the material at a given temperature and frequency.

➤ The problem of temperature separation which was used in the asymmetric sigmoid approach in order to find the frequency shift factors is resolved here.

➤ This technique uses a unique function with seven parameters for the simulation.

➤ As one might notice, there is no available experimental data in the region between the liquid and solid state of the material which is called the transition zone. This fact can reduce the reliability of the fit. In order to have an exact prediction which also covers the transition state of the material, it is necessary to

have some additional data points in this area. This is provided by the bubble inflation experiment, which is explained in the following section.

3.5. Bubble Inflation Technique

The bubble inflation technique yields important information on biaxial membrane stretching. It has been applied here in order to characterize the viscoelastic behavior of HDPE in the transition region between the liquid and solid state. This area is a very important region for thermoforming applications which could not be evaluated in the previous experiments because of limitations of the usual mechanical tests. Pursuant to this, the characterization of the behavior of polymers in this region has been quite lacking.

A bubble was generated on the Monark thermoforming machine at IMI by applying pressure to a preheated flat sheet,. By installing the proper sensors and by characterizing the geometry of the bubble, very important information was obtained in this key region of the forming process, as described in detail in the following sections.

Figure 3.25 illustrates the evolution of the state of the material during the thermoforming process using a typical plot of the elastic modulus. As it is clearly shown in the graph, in this experiment the sheet is inside the oven up to the melting point with a slight overshoot in order to be at the correct forming temperature after exiting the oven. The forming region is located inside the transition state between the solid and liquid state of the material. Therefore, the bubble was constructed right after the exit of the oven in order to characterize the viscoelastic properties in this important region.

This section also includes the modified curve for the elastic modulus after adding the newly calculated data points for the transition state.
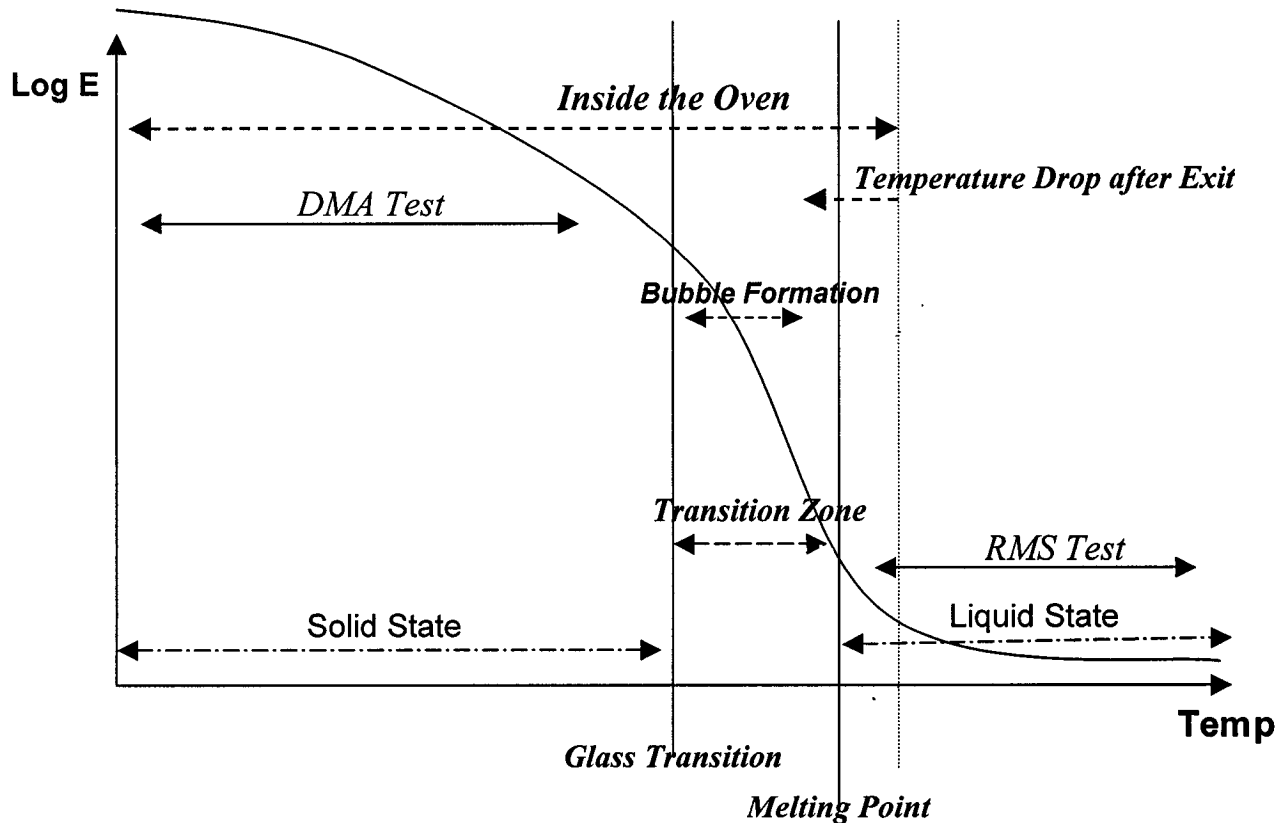
Figure: *3.25 Different states of the material during the thermoforming process*

3.5.1. Experimental Setup

The rectangular preheated sheet, clamped on its sides was blown into a bubble by applying a constant pressure. Figure 3.26 shows the different sensors installed on the Monark thermoforming machine for this experiment. Two position laser sensors were

used, one in a vertical and the other one at an angle, in order to have a better definition of the bubble shape. Pressure was measured with two sensors, one for the blowing period and one for the vacuum stage. An IR thermometer measured the temperature of the surface of the bubble during the experiments.
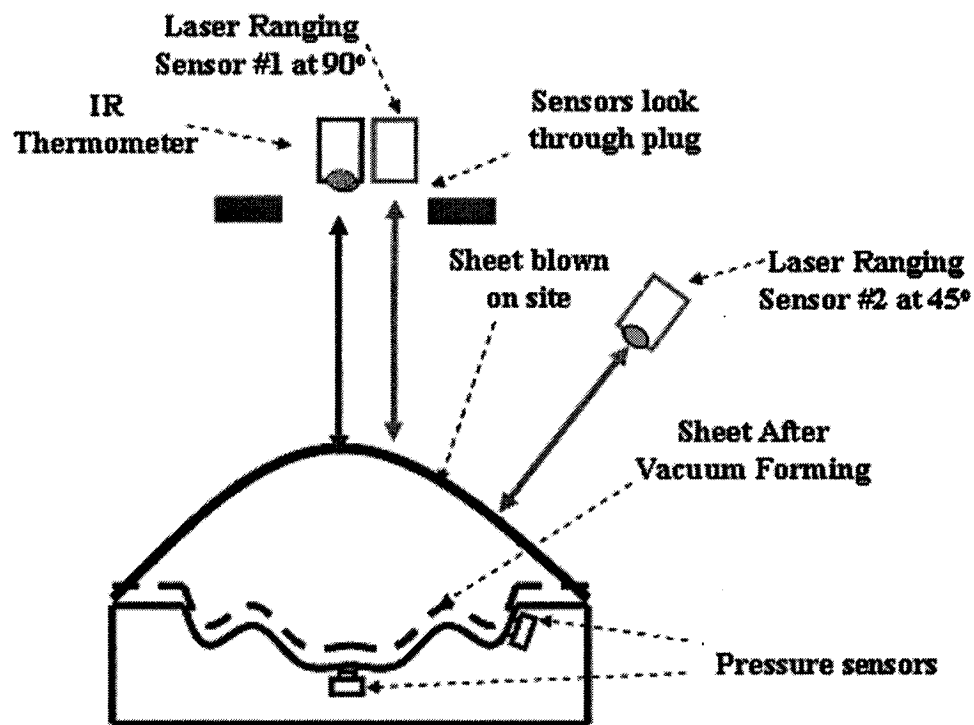
Figure 3.26: Forming stage instrumented for material characterization

Appendix A.2 shows the list of experiments which were done on HDPE with different specifications. Experiment four was chosen because in this experiment the sheet was heated up to 190 °C, which was in a good temperature zone after exiting the oven since the transition state is between 130 and 150°C. A low pressure of 15 PSI was applied

in order to make the bubble, which helps to have a better deployment of the bubble. A circular frame with a radius of 49 cm was used in order to obtain a spherical bubble.

Table 3.9 *Experimental setup for the bubble formation experiment*

Experimental Parameters for Bubble Formation_Exp.#04	
Material Type	HDPE_BA50-100
Sheet Thickness	0.635 CM
Sheet Width and Length	117CM x 117CM
Radius of Circular Rim	49 CM
Applied Pressure	15 PSI
Duration of Applying Pressure	3 Sec
Oven Exit Temperature	186 °C
Heating Time Inside the Oven	540 Sec

3.5.2. Neo-Hookean Relationship

Considering the biaxial extension of a rubbery solid membrane of initial thickness h_0 and radius a, inflated with a differential pressure P. The extensional stress-strain equations for a Mooney-type polymer are [26]:

Eqn. 3.26 $\qquad \sigma_l = 2\left(C_{10} + C_{01} \cdot \lambda_\theta^2\right) \cdot \left(\lambda_l^2 - \frac{1}{\lambda_l^2 \cdot \lambda_\theta^2} \right)$

Eqn. 3.27 $\qquad \sigma_\theta = 2\left(C_{10} + C_{01} \cdot \lambda_l^2\right) \cdot \left(\lambda_\theta^2 - \frac{1}{\lambda_l^2 \cdot \lambda_\theta^2} \right)$

where C_{01} and C_{10} are Mooney constants, and l and θ are in-sheet and angular coordinates (Figure 3.27). N is the force acting on the membrane, $N = \sigma \cdot h$, σ is the local stress and h is the local thickness. The radius from the center axis is r, $\lambda_h = h/h_0$, $\lambda_\theta = r/r_0$, and $\lambda_l = (\lambda_h \cdot \lambda_0)^{-1}$. The angle of the membrane from the horizontal is β and δ is the cap height above the horizontal plane. Thus, $r/R = Sin\beta$, where R is the radius of the spherical cap (Figure. 3.28).

At the top of the dome:

Eqn. 3.28 $\quad \lambda_h = \dfrac{h}{h_0} = \dfrac{1}{1 + (\delta/a)^2}$

For $C_{01} \ll C_{10}$ and $\lambda, \lambda_h \gg 1$, or for large deformations of a neo-Hookean solid:
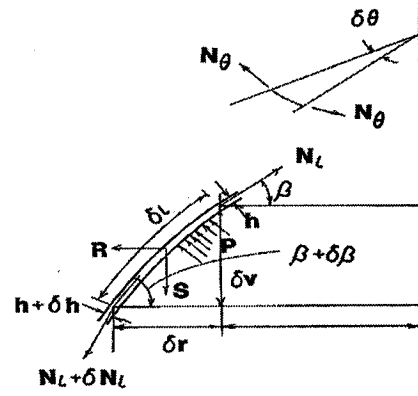
Eqn. 3.29 $\quad \sigma_l \approx 2C_{10} \cdot \lambda_l^2$

Figure 3.27: Membrane stretching geometry[26]

Eqn. 3.30 $\quad \sigma_\theta \approx 2C_{10} \cdot \lambda_\theta^2$

The forces acting on the surface of the membrane are:

Eqn. 3.31 $\quad N_l = \sigma_l \cdot h = \dfrac{\sigma_l \cdot h_0}{\lambda_l \cdot \lambda_\theta} \approx 2C_{10} \cdot h_0 \cdot \left(\dfrac{\lambda_l}{\lambda_\theta}\right)$
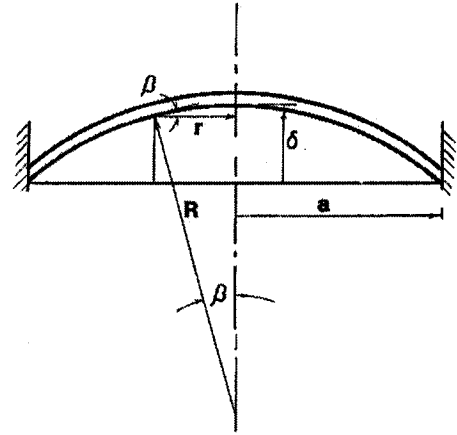
Figure 3.28: Geometry of stretched cap[26]

Eqn. 3.32 $\quad N_\theta = \sigma_\theta \cdot h = \dfrac{\sigma_l \cdot h_0}{\lambda_l \cdot \lambda_\theta} \approx 2C_{10} \cdot h_0 \cdot \left(\dfrac{\lambda_\theta}{\lambda_l} \right)$

Now, $N_l \cdot N_\theta = (2C_{10} h_0)^2 = N_0^2$, a constant. Further, stress equilibrium yields $N_l = N_0$.

Therefore, $N_\theta = N_l$. A hoop stress condition is:

Eqn. 3.33 $\quad \dfrac{\sigma_l h_0}{N_l} = \dfrac{PR}{2}$

As a result:

Eqn. 3.34 $\quad \sigma_l = \lambda_l^2 \cdot \dfrac{PR}{2h_0} \approx 2C_{10} \cdot \lambda_l^2$

And since $R = R(a, \delta)$ above:

Eqn. 3.35 $\quad \dfrac{Pa}{2h_0} \approx \dfrac{4C_{10}(\delta/a)}{1 + (\delta/a)^2} = \dfrac{4E(\delta/a)}{1 + (\delta/a)^2}$

where E is the elastic modulus of new-Hookean polymer. This equation is called the *Neo-Hookean relationship* between applied pneumatic pressure, P, and the extent of deformation, given as δ/a.

3.5.3. Correction of the Generated Curve for Elastic Modulus

The elastic modulus (E) can be obtained from Eqn. 3.36.

Eqn. 3.36 $\quad E = \dfrac{Pa\left(1 + (\delta/a)^2\right)}{8h_0(\delta/a)}$

From the experimental results, we have the values for pressure and the bubble height

during the bubble formation, thus the values for E can be generated (Table 3.9).

Table 3.10: Calculated values for the elastic modulus applying the New-Hookean

relationship

Time	Pressure	Temp.	E(t)	E(t)	E(t)
Sec	PSI	C	PSI	MP	Log_MP
639.6	0.7987	144.1640	15.4208	0.1063	-0.97336
640.1	1.1988	143.1650	23.2709	0.1605	-0.79465
640.6	1.1592	143.8550	23.0322	0.1588	-0.79913
641.1	1.7262	143.1650	34.6694	0.2390	-0.62152
641.6	2.2773	143.2560	45.9774	0.3170	-0.49892
642.1	2.8337	143.1650	57.6351	0.3974	-0.40078
642.6	2.4679	142.8570	50.2003	0.3461	-0.46076
643.1	3.5304	141.9680	71.9248	0.4959	-0.30459

The data values in bold are the three average points that are added to the new plot

for elastic modulus. Table 3.10 shows the newly added points for the elastic modulus

graph. These three generated data points were added to the graph of the elastic modulus

at three frequencies.

Table 3.11: New generated points for the elastic modulus graph obtained by the bubble inflation technique

Point	Temp.	E(t)
	°C	Log_MP
1	144.1640	-0.97336
2	143.1650	-0.62152
3	141.9680	-0.30459
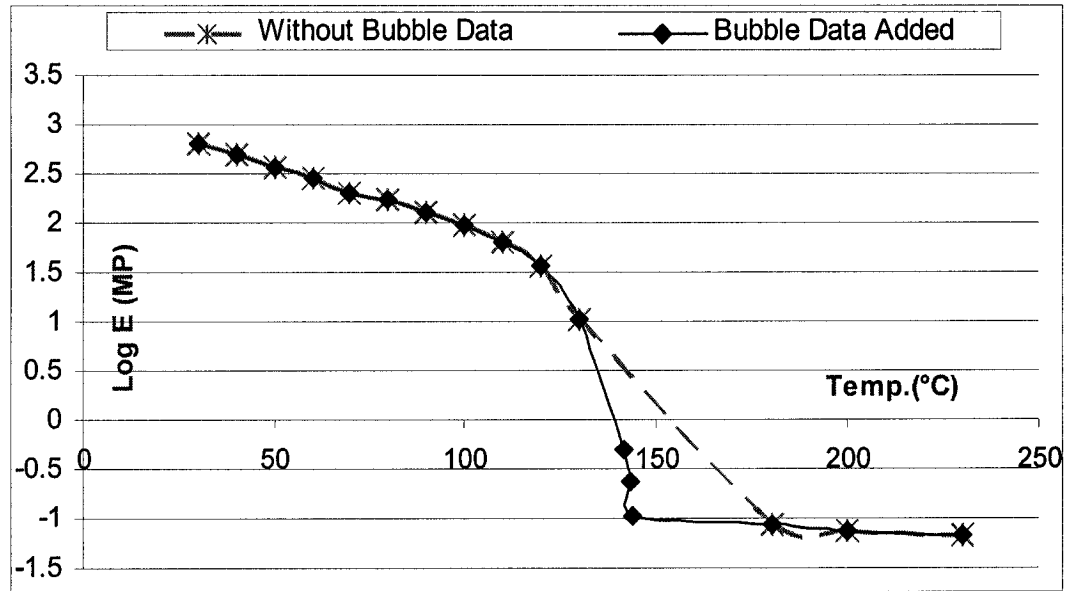
Figure 3.29: *Comparison of the graphs of the elastic modulus before and after adding*

the new points obtained from the bubble inflation experiment.

As demonstrated in figure 3.29, the newly generated curve shows a completely different behavior in the transition state of the material. This improved curve for the elastic modulus makes for a complete difference in modeling the viscoelastic behavior of the material in a semi-solid state.

3.5.4. Characterization

The newly generated graph was modeled with the Table Curve 2D software. Again, an asymmetric sigmoid model is a good assumption to start with. This assumption was based on the behavior of this mathematical model in $+\infty$ and $-\infty$, which is a perfect match in this case.

The graph in figure 3.30 shows the experimental curve along with the asymmetric sigmoid fit. This model fits the curve with an excellent correlation of 0.99.
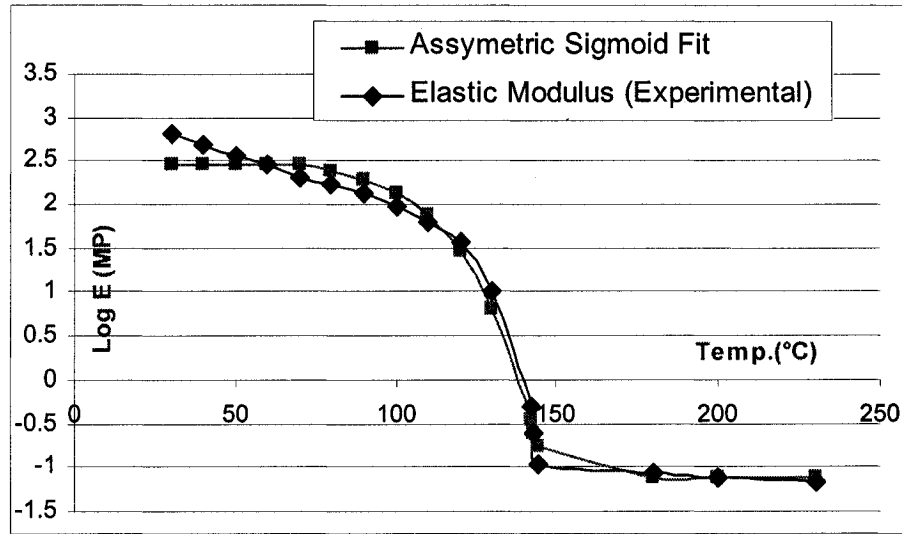
Figure 3.30: *Experimental curve for the elastic modulus along with the asymmetric sigmoid fit after adding the information from the bubble inflation experiment to the original data.*

From equation 3.37 for the asymmetric sigmoid fit, table 3.11 presents the parameters for this experiment.

Eqn. 3.37 $$E' = a_0 + \frac{a_1}{\left(1 + \exp\left(-\dfrac{T - a_3 \ln\left(2^{1/a_4} - 1\right) - a_2}{a_3}\right)\right)^{a_4}}$$

Table 3.12: *Parameters for the asymmetric sigmoid equation*

a_0	a_1	a_2	a_3	a_4
2.561	-3.679	131.213	0.116	0.005

3.5.5. Conclusions with respect to the bubble inflation technique

➢ By applying the bubble inflation technique, additional insight into the viscoelastic behavior of HDPE in the important transition or semi-solid state was obtained.

➢ No similar results for the prediction of the viscoelastic behavior in the transition or the semi-solid area can be found in the literature for polymers.

➢ The newly generated curve covers the behavior of the elastic modulus during the whole thermoforming process.

➢ The forming stage occurs in the transition zone between the liquid and solid state and the bubble inflation technique provides a better characterization of the material's behavior in this area, which translates into better simulation predictions and process control, especially with regard to part thickness and sag in oven.

CHAPTER 4. Characterization of the Level of Frozen-in Stresses

4.1. Introduction

Frozen-in or residual stresses in polymeric materials are mainly caused by the mechanical processes used in manufacturing. In the case of polymer sheets used in thermoforming applications, this process is calendering.

Calendering is a surface finishing process in which a material is drawn between rollers or plates mostly to transform it into sheets of uniform thickness and/or width, or to make the surface smoother. The applied force during this process creates the residual stresses inside the sheet. Since the sheet is cooled rapidly afterwards, some of these stresses cannot be relaxed and remain as "frozen-in" stresses.

Even two polymer sheets from the same batch can have different levels of frozen-in stresses. This variation in the level of frozen-in stresses can cause different behavior of the sheet during the heating stage of the material which can affect the final quality of the manufactured part. This shows the importance of the characterization and detection of these frozen-in stresses during the thermoforming process in order to have a finished part of uniform thickness and to decrease the thickness variation in different manufactured parts.

In this paper, the level of frozen-in stresses is characterized by heating the sheet above the glass transition temperature and comparing the rate of sag as the sheet heats up. Therefore, a close monitoring of sag during sheet heating is done and to the heating process is simulated. The maximum amount of sag during the heating stage is directly related to level of frozen-in stresses inside the sheet. During the heating process and after

the temperature passes the glass transition temperature the residual stresses start to relax, which causes shrinkage of the sheet and therefore affects the amount of sheet sag.

Not taking into account the sheet's frozen-in stresses in the thermoforming process will cause either excessive or insufficient sag, which may result in localized webbing, non-uniform sheet temperature and non-uniform thickness. Therefore, characterization of the level of frozen–in stresses and its direct consequence, sag, is an important indicator of part quality. Since the amount of sag modifies the distance from the sheet to the heating elements, accurate prediction of sag is of primary importance for the thermoformer and part designer [28].

4.2. Prediction of Thermoforming Sag by Simulation

When a polymer sheet clamped in a frame is heated, it begins to sag elastically under its weight. As the temperature increases, the relaxation of frozen stresses in the material starts. The rate of sag varies as the sheet temperature continues to increase.
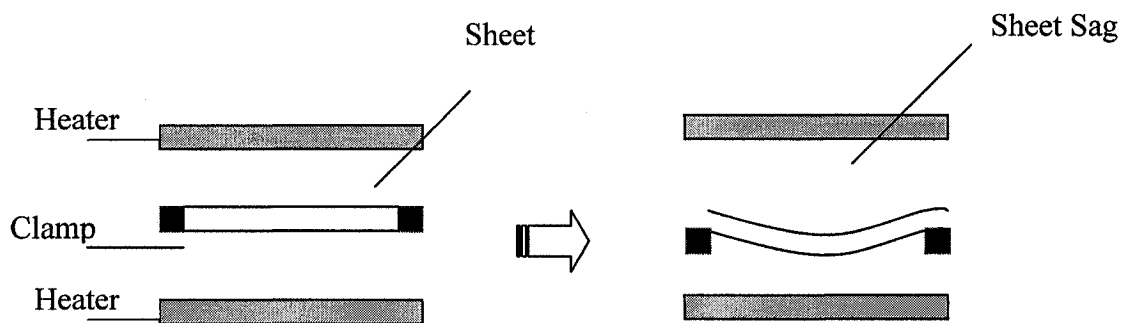

Figure 4.1: Schematic of sheet sag inside the thermoforming oven

Modeling of the thermoforming process has made great strides in recent years; however, due to its complex nature, sheet sag behavior is still an area where simulation precision can be improved [29].

In this section, a series of experiments are presented that allow characterizing this phenomenon. Also, some models for sag prediction are developed and evaluated by comparison with experimental results.

4.2.1. Experimental Setup

As explained in chapter 2.3, all of the experimental measurements were performed on a Monark industrial scale thermoforming machine at the IMI's facilities. HDPE (high density polyethylene), manufactured by Exxon, grade BA50-100 sheets of 1.170m by 1.170m were used. Only oven B was used. It has two heater banks with ceramic elements for profiled control of twenty four zones per side. The Sheet thicknesses were 6.35mm and 9.25mm. For this study the temperature of the top and bottom heaters was set uniformly at 330 °C. Appendix A.2 describes the details of all the experiments done on the Monark machine with HDPE sheets.

A Lauze 96mv 5071-421 laser-ranging sensor was used to measure the sag at the center of the sheet. Also an infrared thermometer (IRT) was used to measure the surface temperature of the sheet.

A correction for the recorded temperatures was required as IR radiation reflected from the sheet's surface was found to influence the IRT signal. Equation 4.1 was used to correct the recorded temperatures.

Eqn. 4.1 $Corrected\ IRT\ output(°K) = \left(T_{read}^4 - \left(T_i^4 - T_a^4\right)\right)^{0.25}$

where T_{read} is the temperature read by the IRT in degrees Kelvin, T_i is the initial temperature in degrees Kelvin read by the IRT on the entry of the sheet into the oven and T_a is the actual sheet temperature on entry in degrees Kelvin. Figure 4.2 shows the original and corrected IRT values as measured on the surface of the sheet. This on-line correction represents the amount of energy that is reflected from the sheet surface and can be used to tune this specific aspect of the simulation.

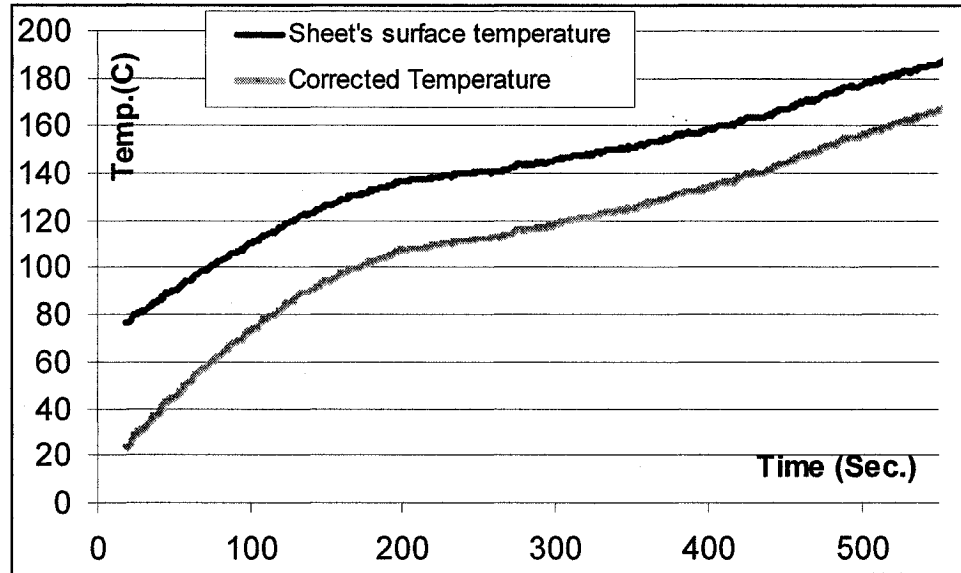*Figure 4.2: Sheet's measured and corrected surface temperature inside the oven*

4.2.2. Experimental Results

After doing several experiments on the Monark machine(Appendix 2), applying the correction for the recorded temperatures and calibrating the recorded data by the sag sensor, the following results were deducted. (A moving average of the recorded data was used because of the large number of data points)

77

Plotting sag vs. time and sag vs. temperature for the different experiments, shows two different types of behavior for the conducted experiments. Figures 4.3 and 4.4 show the first type of results which was obtained from experiments 1 and 3. (A.2)

As it is clearly seen in figure 4.3, two transition points can be identified on the sheet experimental sag curve. Segment 1 shows the linear behavior of the sag at the beginning, when it reaches the glass transition temperature (about 110 °C), where the first transition occurs. The first transition can be attributed to the exterior layer of the sheet passing through the melt transition temperature [29] which is the beginning of the relaxation phenomenon. The second segment of the curve indicates the temperature range in which frozen-in stresses are being released. In this range, there is no significant change in the amount of recorded sag. This is caused in this particular case by the shrinkage of the sheet caused by relaxation phenomenon, which counteracts the sag.
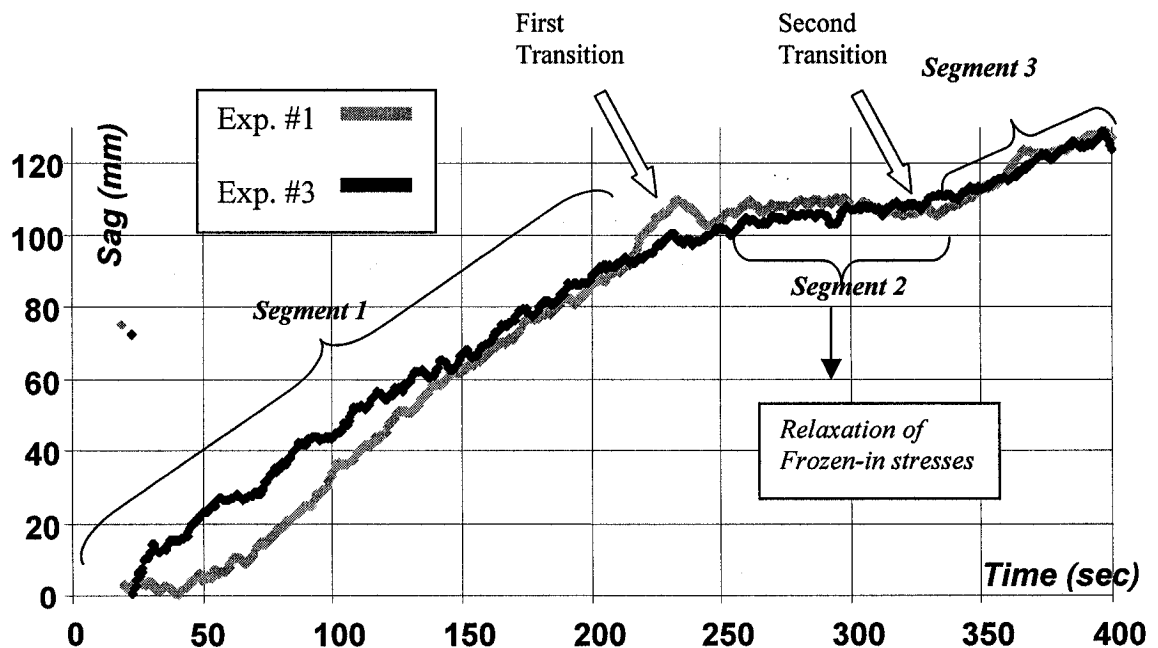

Figure 4.3: *Sag versus time plot for HDPE (6.35 mm thickness) with both sides heated*

for the results from experiments 1 and 3

After the relaxation of all the frozen-in stresses, a second transition occurs. The second transition can be attributed to the interior layers entering the molten state [29] and this is the place where relaxation is complete and all the residual stresses are released. The sheet sag increases again after the second transition in a linear manner (segment 3), up to the maximum sag point occurring at the melting point of HDPE (between 130 °C and 140 °C). A maximum sag of 130 mm was recorded during this experiment.
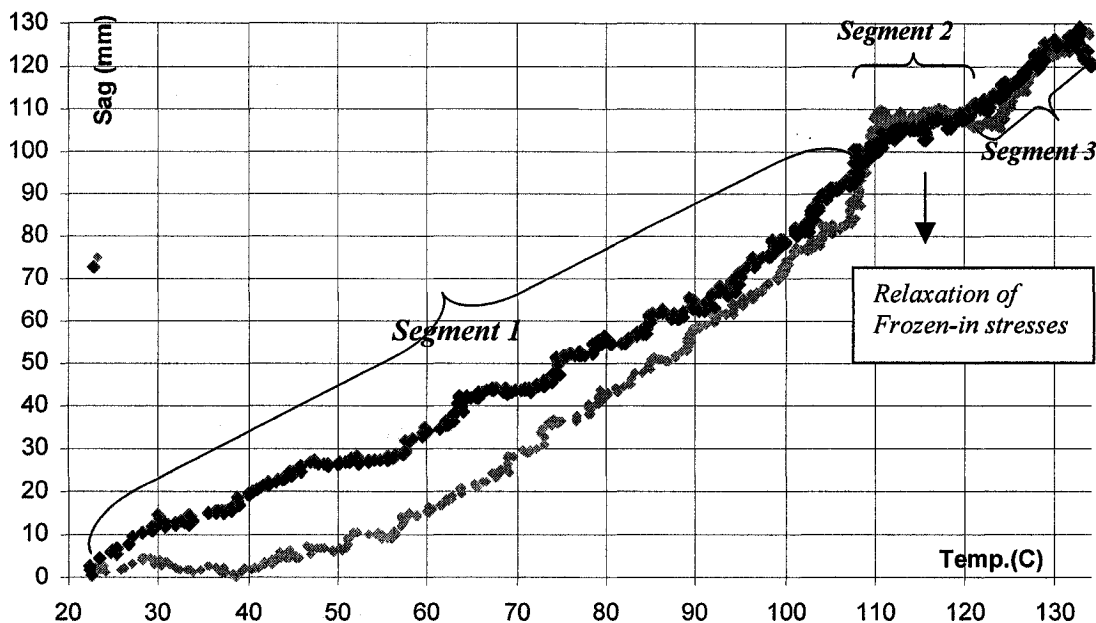

Figure 4.4: *Sag versus temperature plot for HDPE (6.35 mm thickness) with both sides heated for the results from experiments 1 and 3*

Figure 4.5 shows the second type of experimental results for HDPE with a sheet thickness of 6.35 mm for experiments 4, 5, 6 and 7 (appendix 2). As can be seen, no

significant transition can be identified on this graph and it behaves linearly during the whole heating process. Based on the previous theory, this shows that we had no significant amount of frozen-in stresses in the sheets used for these experiments.
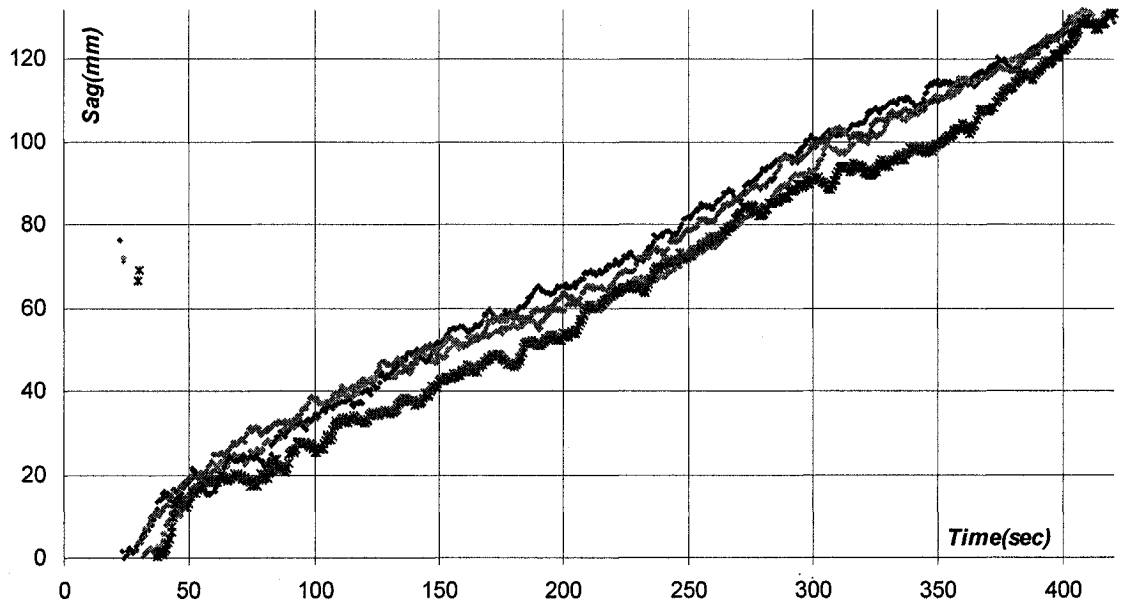
Figure 4.5: Sag versus time plot for HDPE (6.35 mm thickness) with both sides heated

for the results from experiments 4,5,6 and 7

After reviewing the experiment logs it was found that these particular sheets had been used in a previous experiment which was stopped after heating for a short period, due to a technical problem. The material was obviously heated enough to reach the glass transition temperature and to relax the frozen-in stresses. This allowed us to visually compare the two sheets with high and low levels of frozen stresses (Figure 4.6).
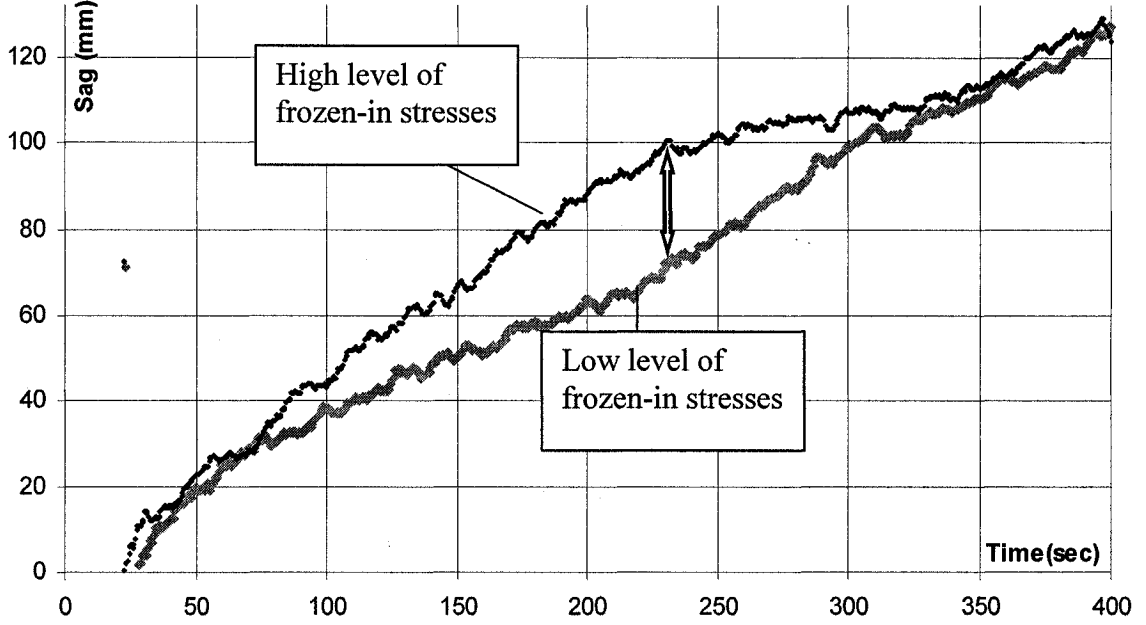
Figure 4.6: *Comparison of the sag phenomenon in two sheets with different levels of frozen-in stresses*

4.2.3. Numerical Approach used in the Simulation

One of the numerical approaches used to characterize sag is based on the KBKZ rheological model [29]. This model was originally used to predict the large deformations during the forming stage. It was modified to extend its validity in order to predict sheet sag during the heating stage of the process. Equation 4.2 represents this model.

Eqn. 4.2 $$\sigma(t) = -qId + \frac{1}{1-\theta} \int_{-\infty}^{t} \frac{g_k}{\tau_{k,\tau}} \exp\left(-\frac{(t-\tau)}{\tau_{k,\tau}}\right) h_k\left(I_1, I_2\right)\left(c^{-1}(\tau,t) + \theta\, c(\tau,t)\right) d\tau$$

81

This equation gives the true stress tensor σ at time t as a function of the Cauchy strain c, strain invariants I_1 and I_2, relaxation modulus g_k and relaxation times τ_k, a damping function h and a model constant θ.

The damping function h, shown in equation 4.3, is the Papanastasiou model where α and β are material constants.

Eqn. 4.3 $\qquad h(I_1, I_2) = \dfrac{\alpha}{(\alpha - 3) + \beta I_1(\tau, t) + (1 - \beta)I_2(\tau, t)}$

The temperature dependency is defined using the WLF shift function applied to the relaxation times of the KBKZ model. Equation 4.4 shows the shift factor a_T as a function of the material temperature T and the material constants T_{ref}, c_1 and c_2.

Eqn. 4.4 $\qquad \ln(a_T) = -\dfrac{c_1(T - T_{ref})}{c_2 + T - T_{ref}}$

Figures 4.7 shows a comparison between the predicted and measured sag at the sheet center using different number of relaxation times in the KBKZ model for 6.35 mm sheet of HDPE.
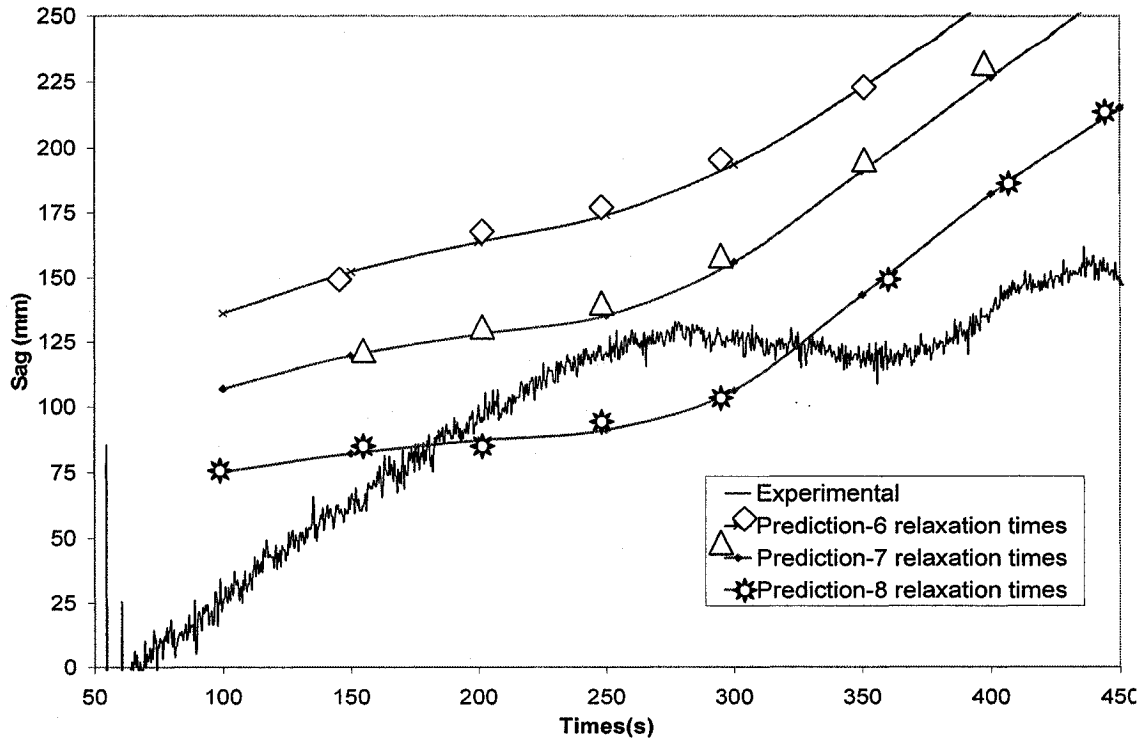
Figure 4.7: Measured and predicted sag for the 6.35 mm thick

HDPE sheet, simulated by KBKZ model[29]

As seen here, using the convocational six relaxation times leads to significant discrepancies between the experimental and numerical results. The material RMS data were fitted again onto the model using seven and eight relaxation times, respectively. Table 4.1 shows the obtained rheological properties for different number of relaxation times.

This study (numerical approach for simulation of the sag) shows that although the modified version of the KBKZ model can improve the prediction of thermoforming sag especially by increasing the number of relaxation times, it is unable to simulate the two identified transition points identified on the experimental graphs.

83

Table 4.1: *Rheological properties for HDPE (Exxon BA50-100) using 6,7 and 8*

relaxation times.

Relaxation spectrum 6		Relaxation spectrum 7		Relaxation spectrum 8	
g_k (MPa)	τ_k (sec)	g_k (MPa)	τ_k (sec)	g_k (MPa)	τ_k (sec)
0.298580	0.004883	0.316738	0.004883	0.184483	0.004883
0.157266	0.039060	0.142424	0.039060	0.145278	0.039060
0.068328	0.312500	0.064539	0.312500	0.063915	0.312500
0.029913	2.500000	0.027625	2.500000	0.027494	2.500000
0.009849	20.00000	0.009049	20.00000	0.009030	20.00000
0.006826	160.0	0.006341	160.0	0.006267	160.0
		20.0	0.0001	56.09146	0.00001
				500.0	0.000001
WLF constants		**WLF constants**		**WLF constants**	
T_{ref}	140.0	T_{ref}	150.0	T_{ref}	150.0
C_1	3.3709	C_1	3.39021	C_1	2.99426
C_2	82.0	C_2	85.0	C_2	70.0

Therefore, this approach cannot be used for the purpose of characterization of the frozen–in stresses, which is closely related to the identification of the transition zones. This is due to the fact that this simulation model does not include the relaxation of the material.

The complexity of the experimental sheet deformation shows that there are still improvements required to accurately model the polymer behavior during the heating phase by applying numerical models. This also shows the necessity of a very accurate

prediction of the temperature profile across the sheet in order to obtain a precise sag predication by applying numerical methods.

4.3. Characterization of frozen-in stresses

As noticed in figure 4.3, there are two transitions. In order to characterize the level of frozen-in stresses, a method needs to be found to characterize these transitions. Figure 4.8 shows the linear fit of different segments of the graph.
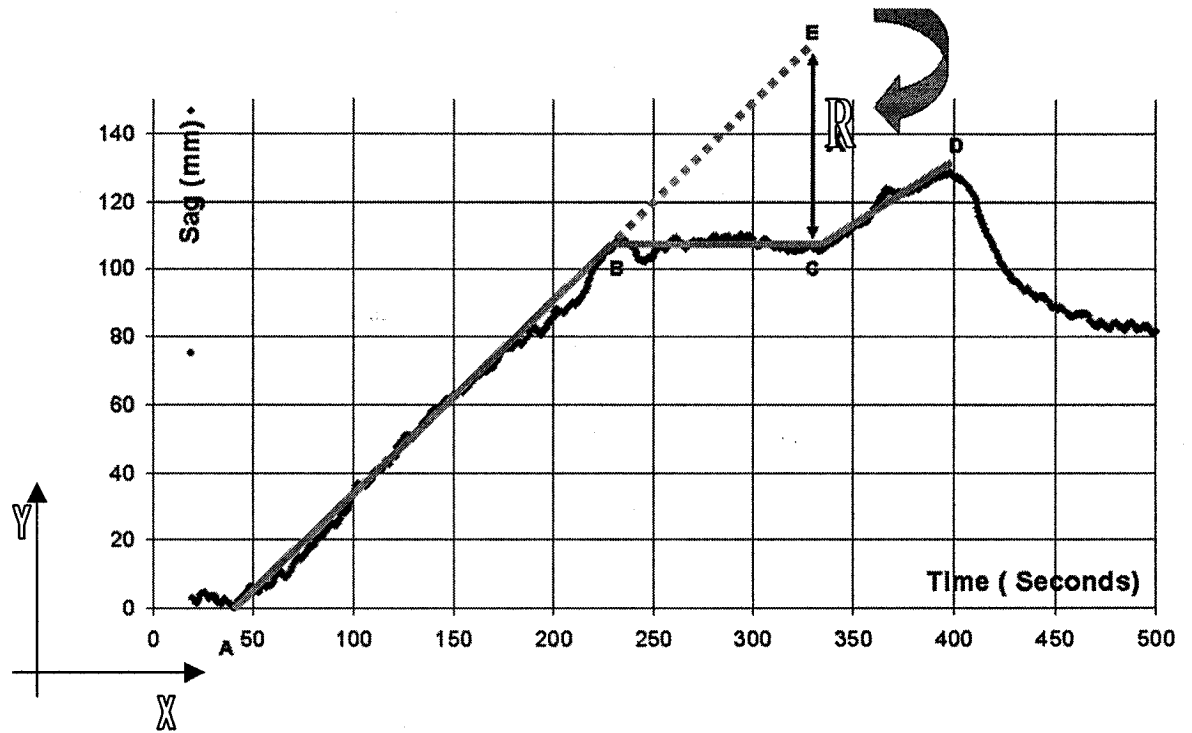

Figure 4.8: Characterization of the level of frozen-in stresses

By developing a simple coding logic, these points can be identified on the experimental graph. Point A is the starting point of sag when y=0. Point B refers to the point where sag stops and there is no considerable variation in the extent of sag ($\delta y \approx 0$,

where δy is variation in y direction). Again point C is the point that sag starts to increase or the variation of sag is again larger than zero (δy>0).

Now, by identifying points A and B, line AB can be characterized. Also point E can be identified as a point on the extension of line AB, which is the point with same magnitude in time axis as point C. Therefore, the distance between points C and E can be identified, which is shown by R in Figure 4.8.

This distance (CE) can be a reference for the level of frozen-in stresses, called *Relaxation Induced Deviation.* By analyzing the data obtained from the sag experiment inside the oven and characterizing the critical points of the transitions in sag, it is possible to characterize during production, the level of frozen-in stresses. This data can then be used in the model based control system.

Also by identifying point D as the maximum sag point, the best forming region for the thermoforming process which is between point C and D can be determined. This is the region after the release of the frozen-in stresses and before the melting point.

CHAPTER 5. Summary, Conclusions and Recommendations

5.1. Research Contributions

This thesis addresses the behavior of the elastic modulus and the relaxation of residual stresses for the material used in the thermoforming process in order to design an online control system. The main motivation of this study was the shortcomings of present simulation models of the thermoforming process in being able to take into account the varying material properties during actual operating conditions, especially from batch to batch. The material properties that were studied included the behavior of the elastic modulus during the whole thermoforming process and also the level of frozen in stresses prior to the actual forming process.

The following are the main contributions of the research describe in this thesis.

1. A technique was developed for on-line characterization of the behavior of the elastic modulus that can be used during the whole thermoforming process.

2. By fitting an asymmetric sigmoid model, a master curve for the behavior of elastic modulus during the thermoforming process was generated. The two parts of the elastic modulus E'' and E' were fitted precisely for the whole temperature range.

3. Using a three dimensional simulation technique, it is now possible to predict the elastic modulus of the material at a given temperature and frequency. It also solves the problem

of the two temperature zones which was required in the asymmetric sigmoid model and reduces the number of dependent parameters for the fit equation.

4. The bubble inflation experiment led to additional insight into the viscoelastic behavior of materials in the important transition or semi-solid state. By applying this technique the previously developed curve for elastic modulus was successfully identified in the vicinity of the transition temperature and the precision of the fit was greatly increased. No similar results can be found in the literature for polymers with regard to the prediction of the viscoelastic behavior in the transition area.

5. A technique for on-line characterization of the level of frozen-in stresses inside the sheet before the forming process was successfully developed. For this purpose sheet sag during the heating stage was closely monitored and characterized.

6. The two developed models for viscoelastic properties and frozen-in stresses address the problems associated with the present simulation model, developed at IMI facility.

7. These two models will be able to adequately represent the material behavior in the process model used in the model based control (MBC) system for the thermoforming process being developed by McGill and IMI.

5.2. Recommendations Future Work

- Finalize the material sub-models.

- Analyze sensitivity of the process to the above parameters in order to minimize the number of parameters that need to be controlled for the process.

- Use the parameters to tune the simulation in order to be able to use it as a soft sensor, for the accurate prediction of the sheet internal temperature profiles for example.

- Generate the local sensitivity matrix from above. This matrix can then be used to adjust the process in-cycle, since its response time is very fast and the required corrections only need to be applied in the vicinity of the operating point, which allows for linear corrections to be used.

- Implement control and diagnostics system using the above.

Acknowledgments

Bibliography

[1] Joseph Fred Chabot, JR. *"The Development of Plastics Processing Machinery and Methods"*, John Willy and Sons, INC., 1992

[2] James L. Throne. *"Technology of Thermoforming"*, Hanser Publishers, 1996, pp. 7-8.

[3] James L. Throne. *"Technology of Thermoforming"*, Hanser Publishers, 1996, Preface.

[4] J. Florian, *"Practical Thermoforming: Principles and Applications"*, Marcel Dekker, New York, 1996, pp.54-57.

[5] A. Illig, *Thermoforming: A Practical Guide*, Hanser Publishers, Munich, 2000, pp.17.

[6] J. Throne, *Technology of Thermoforming*, Hanser Publications, Munich, 1996, pp.114.

[7] A. Illig, *Thermoforming: A Practical Guide*, Hanser Publishers, Munich, 200, pp.19-20.

[8] J. Throne, *Technology of Thermoforming*, Hanser Publications, Munich, 1996, pp.198.

[9] J. Florian, *Practical Thermoforming: Principles and Applications*, Marcel Dekker, New York, 1996, pp.89.

[10] J. Throne, *Technology of Thermoforming*, Hanser Publications, Munich, 1996, pp.16.

[11] A. Illig, *Thermoforming: A Practical Guide*, Hanser Publishers, Munich, 2000, pp.24.

[12] G. Gruenwald, *Thermoforming: A Plastics Processing Guide*, Technomic Publishing CO., Lancaster, 1987, pp57.

[13] J. Florian, *Practical Thermoforming: Principles and Applications*, Marcel Dekker, New York, 1996, pp.99.

[14] J. Florian, *Practical Thermoforming: Principles and Applications*, Marcel Dekker, New York,

1996,   pp.135.

[15] G. Gruenwald, *Thermoforming: A Plastics Processing Guide,* Technomic Publishing CO., Lancaster, 1987, pp.117-125.

[16] J. Florian, *Practical Thermoforming: Principles and Applications,* Marcel Dekker, New York, 1996, pp.90.

[17] J. Florian, *Practical Thermoforming: Principles and Applications,* Marcel Dekker, New York, 1996,   pp.126.

[18] J. Florian, *Practical Thermoforming: Principles and Applications,* Marcel Dekker, New York, 1996,   pp.93.

[19] MX. Berins, *SPI Plastics Engineering Handbook,* Kluwer Academic Publishers, Boston, 1991, pp.385.

[20] J. Florian, *Practical Thermoforming: Principles and Applications,* Marcel Dekker, New York, 1996, pp.130.

[21] G. Gruenwald, *Thermoforming: A Plastics Processing Guide,* Technomic Publishing CO., Lancaster, 1987, pp.122.

[22] A. Dlig, *Thermoforming: A Practical Guide,* Hanser Publishers, Munich, 2000, pp.74.

[23] J. Florian, *Practical Thermoforming: Principles and Applications,* Marcel Dekker, New York, 1996, pp.142.

[24] M.L. Berins, *SPI Plastics Engineering Handbook,* Kluwer Academic Publishers, Boston, 1991, pp.394.

[25] J. Florian, *Practical Thermoforming: Principles and Applications,* Marcel Dekker, New York, 1996, pp.150.

[26] James L. Throne. "*Technology of Thermoforming*", Hanser Publishers, 1996, pp. 282-283.

[27] Alexander Ya. Malkin. "Rheology Fundamentals", Chemtec Publishing,1994

[28] James L. Throne. "*Technology of Thermoforming*", Hanser Publishers, 1996

[29] P.Debergue; P.Girard. " Improving the Prediction of Thermoforming Sag in Simulations Through Experimental Validation of the Transition Model" ,IMI-NRC/CNRC Publications, 2003

Appendix I

E' and E'' experimental data for HDPE BA 50-100, provided by IMI rheological laboratories.

Temp °C	E`(10Hz)_MPa	E'(1Hz)_MPa	E'(0.1Hz)_MPa
30	699.03670	644.21800	560.31980
40	567.50018	488.95287	389.35340
50	459.44444	370.62439	287.57690
60	364.41815	283.96774	218.22274
70	215.44479	197.09109	147.66379
80	214.48849	169.60279	127.13555
90	173.60691	131.65398	99.23686
100	124.92029	93.64207	70.75661
110	87.23685	64.60052	48.31522
120	52.38416	37.22888	29.97878
130	14.76386	10.33021	8.04935
180	0.25215	0.08727	0.02586
200	0.21813	0.07548	0.02389
230	0.18603	0.06732	0.02418

Temp °C	E''(10Hz)_MPa	E''(1Hz)_MPa	E''(0.1Hz)_MPa
30	31.85270	58.04422	80.27510
40	43.58409	65.38935	72.40670
50	50.69207	62.51209	58.99144
60	51.65020	53.14923	46.85242
70	36.72612	38.75476	32.95862
80	37.07780	33.47395	28.58005
90	32.25611	27.21291	23.38676
100	24.42193	20.21734	16.38015
110	17.48807	14.32409	10.31528
120	10.87146	8.31321	5.86885
130	3.45720	2.42209	1.88194
180	0.18951	0.07602	0.02799
200	0.16701	0.06585	0.02233
230	0.13863	0.05535	0.01960

Appendix II

List of experiments done on HDPE with different specifications.

Material – HDPE BA 50-100 1/4"

			Exp1	Exp2	Exp3	Exp4	Exp5
Heating Time	(ref. 160°C)	383sec	X	X	X		X
	(ref. 190°C)	540sec				X	
Zone Heating	Lower Oven		X	X	X	X	X
	Upper oven		X	X	X	X	X
Bubble pressure							
L:	3sec	15PSI					
S:	5sec	60PSI	X	X	X	X	X
H:	3sec	60PSI					
Plug Assist	Vacuum						
	Plug and Vacuum		X	X	X	X	X
	Bubble, Plug and Vacuum						
Sheet & File #:			BPV19017_05H1	BPV16018_05H2	BPV19025_05S3good	BPV19023_06L4resisfinal	V19021_065good
Sheet & File #:							
Sheet & File #:							

Nomenclature of File Names: BPV19019_05H1

BPV = Plug Assit (V: Vacuum only / PV: Plug and Vacuum / BPV: Bubble, Plug and Vacumm)
190 = Sheet temperature
19_05 = Date (Day & Month)
H = Bubble pressure (H=high, L=low, S=slow)
1 = Experiment Number

Legend
good:
no good:

Material - HDPE BA 50-100 1/4"

		Exp6	Exp7	Exp8	Exp9	Exp10
Heating Time						
(ref: 160°C)	383sec	X	X			
(ref: 190°C)	540sec			X	X	
Zone Heating						
Lower Oven		X	X	X		
Upper oven		X	X		X	
Bubble pressure						
L : 3sec	15PSI		X			
S : 5sec	60PSI	X				
H : 3sec	60PSI			X	X	
Plug Assist						
Vacuum						
Plug and Vacuum						
Bubble, Plug and Vacuum		X	X	X	X	
Sheet & File #:		BPV16000__06S6	BPV16016__06L7	BPV19029_06H8	BPV19029_06H9	
Sheet & File #:		BPV16019_06S6good	BPV16023_06L7good			
Sheet & File #:		BPV16021_06S6final				

Nomenclature of File Names: BPV19019_05H1

BPV = Plug Assit (V: Vacuum only / PV: Plug and Vacuum / BPV: Bubble, Plug and Vacumm)
190 = Sheet temperature
19_05 = Date (Day & Month)
H = Bubble pressure (H=high, L=low, S=slow)
1 = Experiment Number

Legend	
good:	
no good:	